Research Paper

GEOSPHERE

GEOSPHERE; v. 12, no. 5

doi:10.1130/GES01349.1

16 figures; 2 tables; 2 supplemental files

CORRESPONDENCE: jbeyer@geo.umass.edu

CITATION: Beyer, J., and Griffith, W.A., 2016, Influence of mechanical stratigraphy on clastic injectite growth at Sheep Mountain anticline, Wyoming: A case study of natural hydraulic fracture containment: Geosphere, v. 12, no. 5, p. 1633–1655, doi:10.1130/GES01349.1.

Received 25 April 2016
Revision received 20 July 2016
Accepted 17 August 2016
Published online 9 September 2016

Influence of mechanical stratigraphy on clastic injectite growth at Sheep Mountain anticline, Wyoming: A case study of natural hydraulic fracture containment

Jennifer Beyer* and W. Ashley Griffith

Department of Earth and Environmental Sciences, Geoscience Building, 500 Yates Street, University of Texas, Arlington, Texas 76019, USA

ABSTRACT

Sandstone injectites ranging from <30 m to >1 km in outcrop length intrude the Cretaceous Mowry Formation in the vicinity of Sheep Mountain anticline (Bighorn Basin, Wyoming, USA). These injectites were sourced from the Peay Sandstone Member of the overlying Cretaceous Frontier Formation and represent a significant possible fluid pathway through impermeable shales. Sand injection occurred along dikes and sills, interacting with bedding discontinuities and preexisting joints in the Mowry Formation during the early folding of Sheep Mountain anticline. We argue that, in contrast to the passive sweeping of sediments into fissures characteristic of Neptunian dike formation, downward intrusion of the Peay sand was forceful and made possible by a highly stratified horizontal stress field resulting from the deposition, burial, and lithification history of the rock units in the area.

The internal structure of the injectites is dominated by two sets of mutually offsetting deformation bands. The deformation bands have shear and compaction components, exhibiting significant porosity loss, as well as cataclasis and minor pressure solution. After formation of the deformation bands, subsequent faulting was localized along the margins of deformation bands, evidenced in the field by slickensided surfaces. A detailed kinematic analysis of slickenline lineations yields shortening and extension axes consistent with deformation band formation during early Laramide–oriented shortening, and continuing through the folding of Sheep Mountain anticline. Beyond the formation and deformation of these sandstone injectites, this study highlights the importance of mechanical stratigraphy in the containment of hydraulic fractures.

INTRODUCTION

Clastic injectites are intrusive bodies of sediment, commonly sand, that cut across lower permeability rocks in a manner analogous to igneous intrusions (Jolly and Lonergan, 2002). Injectites form as dikes and sills in cohesive rocks or more irregular geometries in noncohesive host materials, and they can form at any depth if a source of noncemented sediments can be fluidized. Intrusion can occur in any direction depending on the nature of the local stress field. In glacial environments, injectites commonly intrude downward, but in most sedimentary environments, injectites typically grow upward and laterally (Jolly and Lonergan, 2002). A distinction can be made between injectites, which are true dikes and sills formed as a result of forceful injection, and passive fissure fills, known as Neptunian dikes (Demoulin, 1978; Smart et al., 1988).

Reports of clastic injectites in the geologic literature date back to the 1820s (Braccini et al., 2006), when they were considered geologic oddities. More recently geologists have recognized that clastic injectites occur in nearly all sedimentary environments, although known locations of injectites are perhaps biased toward deep-water marine settings (Jolly and Lonergan, 2002). Clastic injectites have also been found to intrude granitic rock, mafic sills, and pillow basalts (Jolly and Lonergan, 2002; Hurst and Cartwright, 2007). The importance of clastic injectites is being recognized in areas where these soft sediment deformation and intrusion processes directly affect hydrocarbon reservoirs (Braccini et al., 2006). In cases where clastic injectites intrude impermeable units, they act as both seal risks and migration pathways that can potentially increase connectivity between reservoirs isolated by units of low permeability (Jolly and Lonergan, 2002). It has been recognized that a better understanding of clastic injectites and the mechanics of their intrusion could be directly relevant to the recovery of petroleum reserves (Hurst and Cartwright, 2007).

Clastic injectites also serve as examples of large-scale natural hydraulic fractures, in that they propagate as opening mode cracks in the σ_1-σ_2 plane driven by an overpressurized fluid-sand slurry. Hydraulic fractures are generated and driven by internal fluid overpressure that locally exceeds the confining pressure (Gudmundsson, 2002). The propagation of any opening mode fracture in layered rocks can be strongly influenced by mechanical stratigraphy, due to contrasts in mechanical properties between adjacent layers (Bourne, 2003) and the presence of bedding-plane discontinuities (Cooke and Underwood, 2001). For hydraulic fractures to be effective in petroleum recovery, they need to be contained within the reservoir layer. The mechanical properties of the reservoir and sealing formations, and the minimum horizontal in situ stresses in these formations, play important roles in the prediction of fracture containment (Simonson et al., 1978; Bourne, 2003), as does the presence of

*Now at Department of Geosciences, University of Massachusetts, Amherst, Massachusetts 01003, USA

preexisting discontinuities, such as bedding interfaces and joints (Cooke and Underwood, 2001). For example, depending on the strength of the interface, fractures may propagate straight across a depositional contact, step over at the contact, or terminate at the contact (Cooke and Underwood, 2001), and preexisting fractures can either promote or hinder hydraulic fracture propagation, depending on the orientation of the fractures with respect to the prevailing stress field (Warpinski and Teufel, 1987). If joints lack a cement fill, or the tensile strength of the contact between the cement fill and wall rock is weak, the joints can be dilated and promote propagation. If, however, joints are well cemented, hydraulic fractures may terminate at the joints (Gale et al., 2007). The angle at which the incipient fracture intersects the joints will also play a role in fracture propagation, where hydraulic fractures intersecting joints at large angles will likely terminate at the discontinuity and hydraulic fractures intersecting joints at small angles are more likely to dilate the joints (Warpinski and Teufel, 1987). Hydraulic fractures are generally assumed to propagate upward (and laterally) from areas of higher pressure to areas of lower pressure, as both lithostatic compressive stresses and hydrostatic fluid pressure generally increase with depth; however, Simonson et al. (1978) showed that in a homogeneous medium, downward propagation is probable if the fluid pressure gradient is greater than the minimum horizontal in situ stress gradient.

In this study we investigate the formation mechanisms of large sandstone intrusions in the vicinity of Sheep Mountain anticline (SMA), between Lovell and Greybull, Wyoming, USA (Fig. 1). The presence of sand intrusions at SMA was first reported in the early 1900s (see Fisher, 1906), but only Warner (1968) studied their structure in detail. These sandstone intrusions are well exposed in three dimensions (Fig. 2), and some are >1 km in outcrop length. They crop out in the Mowry Formation (Fig. 1), a proven petroleum source rock that is stratigraphically lower than the proposed source rock for the intrusions. We evaluate two potential mechanisms for downward intrusion: (1) forceful downward injection aided by a stratified stress field, and (2) passive sweeping of sediments into open fissures to form Neptunian dikes. Neptunian dikes in the marine realm, or fissure infills in the terrestrial realm, form when sediments passively infill fractures in older strata (Smart et al., 1988). While the intrusions at Sheep Mountain have been interpreted as Neptunian in origin (e.g., E. Erslev, 2014, personal commun.), we present an alternative theory of formation consistent with forceful intrusion by hydraulic fracturing. We also investigate deformation bands within the intrusions, and find that they record deformation after intrusion and aid in reconstructing the relationship between deformation of the intrusions and fold kinematics of SMA.

BACKGROUND

Geography of the Study Area

The study area is located at SMA in the eastern Bighorn Basin, located in north-central Wyoming (Fig. 1). The Bighorn Basin trends northwest-southeast and is bounded by the Bighorn Mountains to the east, the Owl Creek Mountains to the south, the Absaroka Range and Beartooth Mountains to the west, and the Nye-Bowler lineament to the north. SMA is a basement-cored, doubly plunging asymmetric fold that is along the eastern flank of the basin (Johnson et al., 1965; Warner, 1968; Stanton and Erslev, 2002/2003; Bellahsen et al., 2006). SMA trends northwest-southeast and formed subperpendicular to the inferred direction of maximum Laramide orogenic contraction (northeast-southwest), similar to many Laramide-age (latest Cretaceous–early Eocene) folds (Erslev, 1993). The northeastern forelimb dips between 40° and 90° to the northeast, and the southwestern backlimb dips between 10° and 40° to the southwest. The fold plunges as steeply as 20° toward the northwest at the northern extent and ~10° southeast at the southern extent (Bellahsen et al., 2006; Amrouch et al., 2010).

The subsurface geometry of the fold remains relatively unconstrained; however, the fold is interpreted to overlie a southwest-dipping thrust fault (Hennier and Spang, 1983; Forster et al., 1996; Stanton and Erslev, 2002/2003) that was later cut by a northeast-dipping thrust fault (Stanton and Erslev, 2002/2003). An earlier contrasting interpretation of the subsurface geometry involves a southwest-dipping backthrust of an older northeast-dipping thrust fault (Hennier and Spang, 1983; Forster et al., 1996). On the backlimb, a secondary fold branching off the main anticline has been interpreted as a rabbit-ear fold, as defined by Dahlstrom (1969), related to a shallower southwest-dipping thrust fault that merges with the larger southwest-verging thrust fault (Stanton and Erslev, 2002/2003). Amrouch et al. (2010) proposed that the rabbit-ear structure (Fig. 1) is more likely controlled by a deeper basement structure, and suggested that the shallow thrust fault is associated with a triangle zone above a northeast-dipping basement normal fault reactivated as a thrust fault.

Geologic Setting

The Bighorn Basin was located in the Cordillera foreland during the Late Cretaceous and was partitioned into intermontane basins and mountains during the Laramide orogeny in the latest Cretaceous–early Eocene (DeCelles, 2004). By the latest Cretaceous, the effects of Laramide deformation were initiated (Dickinson et al., 1988), and many of the structural elements of the Bighorn Basin began growing at this time. Extensive uplift of the Bighorn Mountains took place in the Paleocene when deformation intensified, and the present-day shapes of the Bighorn Basin and Bighorn Mountains were mostly established by the Eocene (Hoy and Ridgway, 1997; Crowley et al., 2002; Fan and Dettman, 2009; Fan and Carrapa, 2014). There was some volcanism in the Absaroka Range, which extended into the central part of the basin during the middle Eocene (Thomas, 1965), and as volcanism increased into the late Eocene, Laramide deformation gradually decreased until it had nearly ceased (Fanshawe, 1971; Dickinson et al., 1988). The Bighorn Basin was almost completely filled with sediments during the Oligocene and Miocene (McMillan et al., 2006), but by the late Pliocene and early Pleistocene, regional uplift likely resulted in normal faulting and excavation of the Bighorn Basin (Love, 1960; Ray and Keefer, 1985; Byrd et al., 1994).

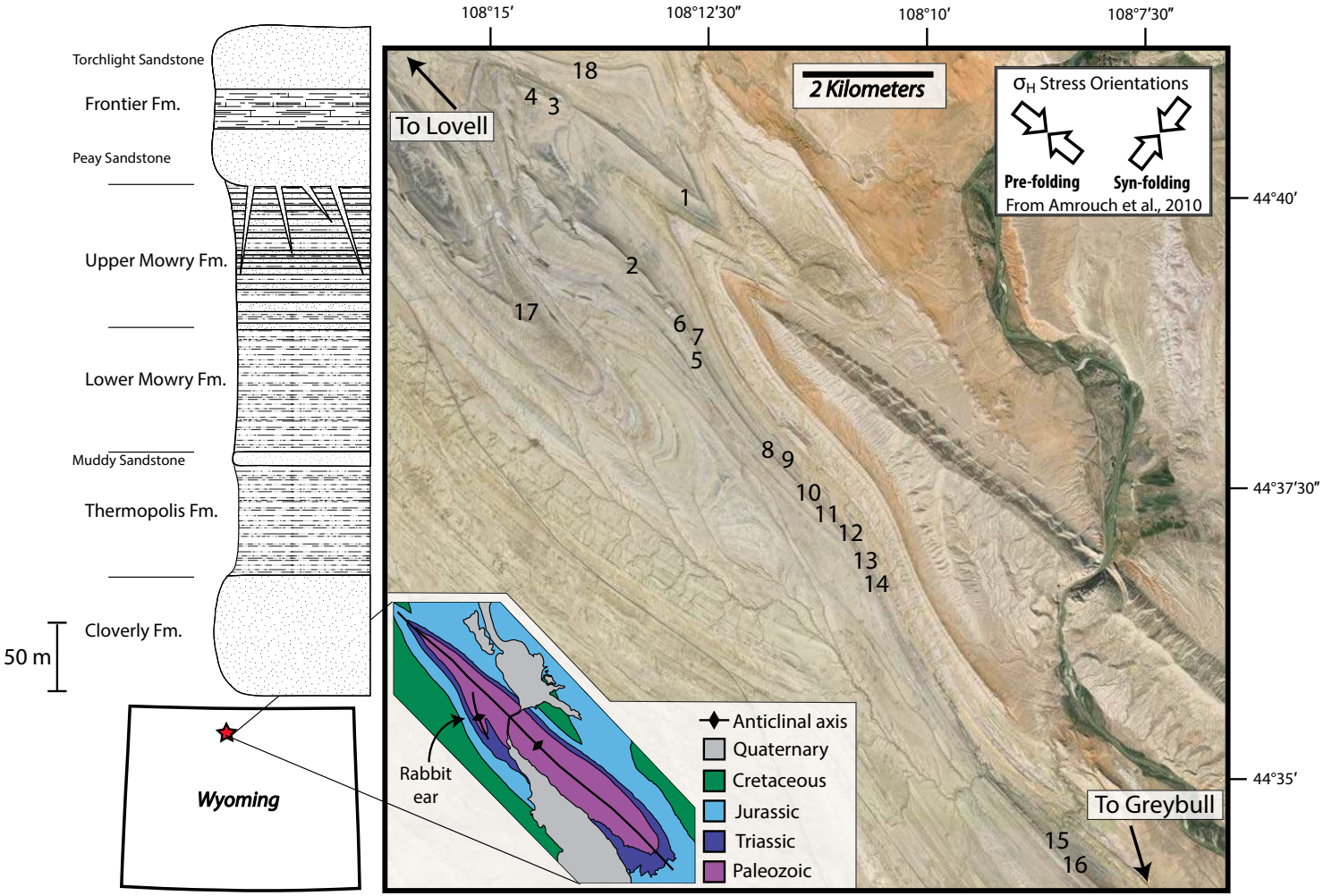

Figure 1. The study area in north-central Wyoming in the Bighorn Basin. This study investigates 18 (numbered) injectites located near Sheep Mountain anticline, an asymmetric anticline that formed during the Laramide orogeny, a northeast-southwest–oriented compressional regime, interpreted from calcite twins, microfaults, and systematic fracture sets in the Madison, Amsden, and Phosphoria Formations and Tensleep Sandstone (Bellahsen et al., 2006; Amrouch et al., 2010). The injectites crop out in the upper Mowry Formation in the lower Cretaceous sedimentary strata.

The injectites at SMA are found within the upper Cretaceous Mowry Formation. The Mowry Formation is 195 m thick and consists of 2 units: a lower section containing gray to black shale with bentonite, and an upper section consisting of ridge-forming light gray to brown siliceous shale with interbedded bentonite and fine-grained sandy units. The Mowry Formation is underlain by the Thermopolis Shale, a 91-m-thick dark gray to black shale with thin bentonite beds; the top of the formation is marked by the white to gray Muddy Sandstone Member. The Frontier Formation, deposited conformably upon the Mowry Formation, is 137 m thick and is divided into three members: the lowermost Peay Sandstone Member, a resistant light gray sandstone; the middle section, a dark gray, silty shale with bentonite; and the upper Torchlight Sandstone Member, a nonresistant light gray sandstone. Above the Frontier Formation is the deeper water Cody Shale, which is 701 m thick (Hennier, 1984).

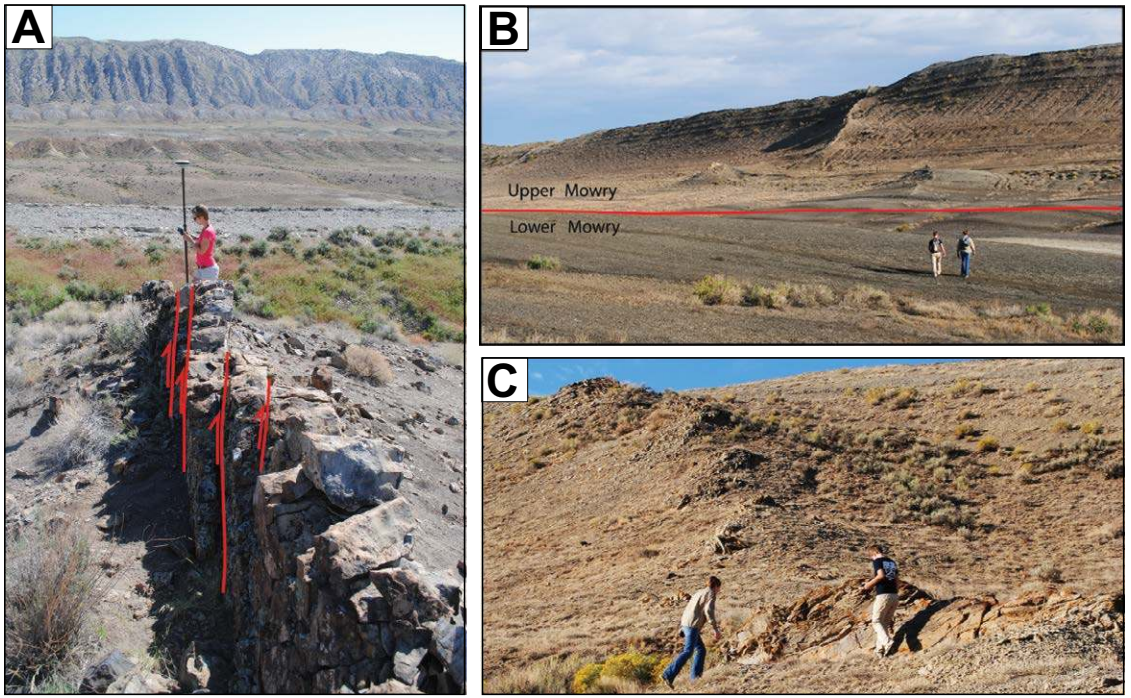

Figure 2. (A) Injectite 10 is ~0.9–1.2 m above the surrounding Mowry Formation. Throughgoing normal faults (n = 14; four highlighted in red) cut the injectite, all of which are parallel to deformation bands. (B) Injectite 1 shows the containment of the injectites to the upper Mowry Formation. Injectites rarely crop out in the Lower Mowry Formation, and do not crop out about the Peay Sandstone Member. (C) Injectite 14 is very weathered, showing very little relief above the Mowry Formation. The injectites are often characterized by en echelon–stepping segments.

Intrusions at SMA: Previous Studies

Warner (1968) mapped a total of 13 sandstone intrusions on the west flank of SMA, reporting observations of fractures, slickensides, and flow patterns within the intrusions, as well as systematic fractures in the surrounding stratigraphic units. In all instances there was at least one systematic joint set in the Mowry Formation that was subparallel to the intrusions (Warner, 1968). Because the Peay Sandstone Member is the nearest sandstone unit stratigraphically (Fig. 1) and is lithologically similar to the intrusion material, Warner (1968) concluded that the Peay Sandstone Member was the most likely source. Furthermore, one of the intrusions mapped extended into the Peay Sandstone Member, and Warner (1968) proposed that downward intrusion occurred during the early stages of the development of SMA.

Mechanics of Upward Intrusion

Natural and artificial hydraulic fracturing requires a sustained pressure differential between the fluid in the fracture and the formation pressure of the surrounding rock in order for the fracture to dilate. In intact rock, the pore fluid pressure must exceed the minimum principal stress plus the tensile strength of the adjacent strata for failure to occur (Vigorito and Hurst, 2010). When the excess pressure dissipates, fracture propagation ceases and the intrusion "freezes" (Jolly and Lonergan, 2002). This is a slight oversimplification, as fracture cessation should occur once the fluid pressure falls below a threshold level such that the stress intensity factor at the fracture tip becomes less than the fracture toughness of the country rock (or cohesive sediment) (Rubin, 1993); however for illustrative purposes, the Jolly and Lonergan (2002) criterion for fracture cessation is reasonable. Excess pressures are most commonly associated with the combined effects of low permeability and rapid burial. This type of overpressure is generally restricted to rock or sediment layers that have been sealed by impermeable caprocks and then rapidly buried (Maltman, 1994), such that the burial rate exceeds the rate at which fluids can escape from the pore spaces, a process referred to as disequilibrium compaction (Jolly and Lonergan, 2002). Before a sand body becomes sealed, the pore fluid pressure (P_f) increases along the hydrostatic gradient (path 0-A [origin to Point A] in Fig. 3B). The P_f will continue to increase along this gradient until the sand body becomes sealed, at which Point P_f will deviate from the hydrostatic gradient and begin to increase along a path parallel to the lithostatic gradient, σ_v (path A-B in Fig. 3B). When P_f overcomes the least compressive horizontal stress (σ_h), the seal fails and a dike forms (Point B in Fig. 3B). The dike propagates upward

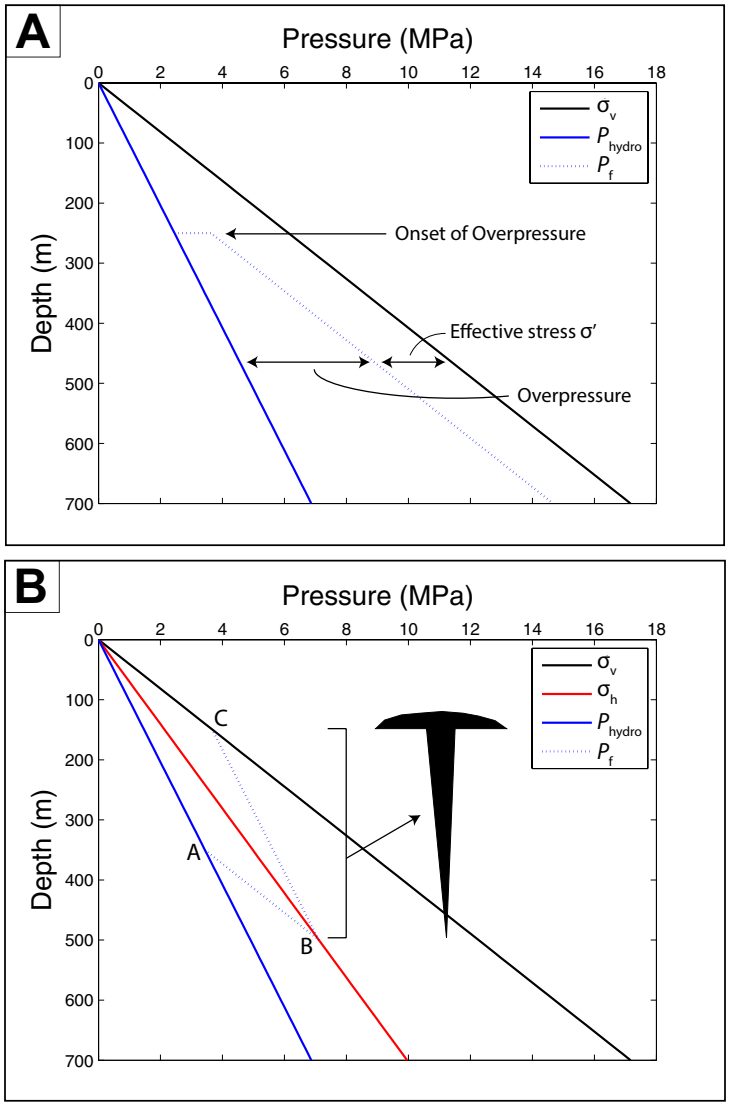

Figure 3. (A) An idealized depth–pore fluid pressure (P_f) path for a sand body that has become overpressured as a result of disequilibrium compaction. (B) Depth–pore fluid pressure path showing the upward intrusion of a dike when the pore fluid (P_f) pressure exceeds the confining pressure (σ_h) at Point B. The dike will continue to propagate until the pore fluid pressure exceeds the lithostatic pressure (σ_v) at Point C, at which time a sill can open (modified from Jolly and Lonergan, 2002).

along the hydrostatic gradient until P_f exceeds σ_v and the intrusion deviates along bedding discontinuities, forming a sill (path B-C in Fig. 3B). This model is consistent with observations of laccolith-shaped sand bodies interconnected with conical sand networks in the North Sea Basin (Rodrigues et al., 2009). In order for flow across the bed to be generated, there has to be a mechanism that imposes a pressure differential rapidly enough for the flow to reach the minimum velocity required to keep the sand grains suspended in flow (Lorenz et al., 1991). When the overpressure in the sand body exceeds the confining pressure, a vertical mode I fracture can form and dilate as it is filled by fluids from the sand body. As the fracture grows, a pressure gradient large enough to mobilize the sand develops at the base of the fracture (Vigorito and Hurst, 2010; Bureau et al., 2014). Other commonly invoked fluidization events are seismicity and localized buildup of excess pressure due to depositional events such as slumping (Jolly and Lonergan, 2002).

While highly idealized, this general model for intrusion provides a mechanical explanation for many of the basic features observed in clastic intrusion complexes; however, the model does not provide a mechanism for downward intrusion. If the interpretation of downward injection of the intrusions at SMA (Warner, 1968) is correct, this requires a modified model. In this paper we first characterize the three-dimensional (3-D) geometry of the intrusions, including their relationships with major structural discontinuities (joints, bedding planes) in the country rock, and we use this information to constrain the kinematics of intrusion and subsequent deformation; deformation bands that are found throughout most of the intrusion segments are key to the latter interpretations. We use high-precision 3-D global positioning system constraints on intrusion geometry to place constraints on in situ stress and fluid pressure gradients during injection, and we present a comprehensive model for intrusion formation at SMA.

METHODOLOGY

We used a Leica Viva global navigation satellite system (GNSS) in a base-rover configuration allowing for real-time kinematic (RTK) corrections to map the 3-D geometry of 18 intrusions around the nose and along the west flank of SMA, achieving a typical accuracy <<2.5 cm (Fig. 1). The presence of intrusions east of SMA is known (E. Erslev, 2014, personal commun.), but these were not mapped in this study. We mapped the contact between the intrusions and beds of the host Mowry Formation by collecting position vectors (Supplemental Tables 1–18[1]) referenced to a Wyoming west-central NAD83 (North American Datum of 1983) coordinate system at approximately regular intervals of 1 m. For well-exposed contacts, a finer spacing was used. We measured the orientation of structural elements (Supplemental Tables 19–36 [see footnote 1], Supplemental Figs. 1–18[2]), including intrusion contacts, joints and bedding in the Mowry Formation, and deformation bands in the intrusions. Where possible, we also collected the slip direction and sense of slip on slickensided surfaces. We prepared blue epoxy-impregnated thin sections of intrusion material and nearby sand bodies (including the Peay and Torchlight Sandstone

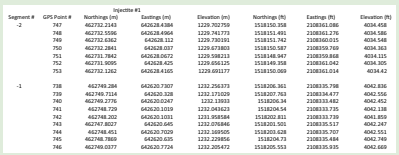

[1]Supplemental Tables. Please visit http://dx.doi.org/10.1130/GES01349.S1 or the full-text article on www.gsapubs.org to view the Supplemental Tables.

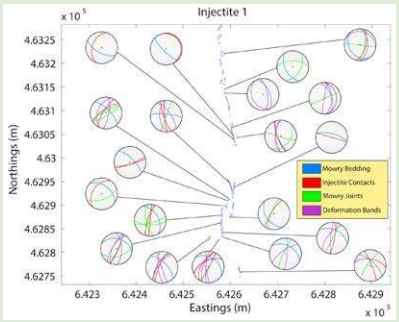

[2]Supplemental Figures. Please visit http://dx.doi.org/10.1130/GES01349.S2 or the full-text article on www.gsapubs.org to view the Supplemental Figures.

Members of the Frontier Formation and the Muddy Sandstone Member of the Thermopolis Shale) for microscopic examination.

We processed the position vector data in MATLAB (http://www.mathworks.com/products/matlab/?requestedDomain=www.mathworks.com) to obtain maps (Supplemental Figures 1–18 [see footnote 2]) of the intrusion outlines in two and three dimensions (Fig. 4). Because the plunge of the SMA fold axis is gentle and the trend is similar to the strike of bedding, we unfolded the structural element orientation data around the local Mowry bedding orientation to obtain the prefolded orientations using Stereonet (Allmendinger, 2015) (Fig. 5). We then performed a kinematic analysis of slip directions (Marrett and Allmendinger, 1990) to determine shortening and extension directions for shearing along deformation bands.

OBSERVATIONS

Geometry of Sandstone Intrusions

The intrusions at SMA are most commonly found in the upper Mowry Formation and very rarely continue downward into the lower Mowry Formation (Fig. 2B). Intrusion 9 was traced upsection into the Peay Sandstone Member of the Frontier Formation, but no intrusions continue more than a few meters into the Peay or extend upward into overlying rocks. The intrusions range in outcrop length from <30 m to >1 km, and maximum apertures range from tens of centimeters to 2 m. All intrusions are segmented along their length, and most segments formed as dikes, crosscutting the local Mowry bedding (Fig. 6A); however, a few segments are sills that are subparallel to and cause flexure of the surrounding Mowry bedding (Fig. 6C). The intrusions are massive, tabular bodies with no apparent internal flow textures, but they commonly contain chert pebbles and deformation bands. The former are similar to pebbles found in the overlying Peay Sandstone Member (Fig. 6G). The intrusions are more resistant to weathering than the surrounding country rock, and the outcrops can vary in appearance from a protruding sand body as much as 2 m above the surrounding rock to piles of rubble arranged in the general trend of the intrusion (Fig. 2C).

Although segmented, the intrusions likely persist at depth as the segments of each intrusion are grouped together with spacing of usually less than a few meters between individual segments, while the spacing between intrusions (each comprising multiple segments) can be at least a few hundred meters. The intrusion segments also show evidence of mechanical interaction where segments overlap and thin near their tips (Figs. 4B, 4C), similar to common observations of large igneous dikes (Delaney and Pollard, 1981). Such segmentation and mechanical interaction is a commonly observed feature along the fringes of opening mode fractures, including dikes, joints, and veins, and is inferred to be related to mechanical interaction and associated local rotations of the principal stresses (Cotterell and Rice, 1980; Delaney and Pollard, 1981; Pollard et al., 1982; Pollard and Aydin, 1988; Cooke and Pollard, 1996).

While present-day intrusion attitudes appear to be nonsystematic (Fig. 7A), unfolded attitudes reveal a more systematic pattern (Fig. 7B). Representative orientations of tabular intrusive bodies are chosen as the average orientation among multiple (sometimes more than 20–30) individual segments (Fig. 5). Upon unfolding, most intrusion segments restore to subvertical orientations, whereas some segments are subhorizontal (Fig. 5B). Those intrusion segments that unfold to horizontal are clearly parallel to the Mowry bedding in the field. The unfolded intrusions can be subdivided into northwest-southeast (Fig. 7C) and northeast-southwest strikes (Fig. 7D). Northwest-southeast–striking intrusions occur in the northwestern backlimb and hinge region of SMA, whereas northeast-southwest–striking intrusions are spread across the entire backlimb and hinge regions (Fig. 7).

Joints in the Upper Mowry Formation

In outcrop, the upper Mowry Formation contains several systematic joint sets cutting both resistant sandstone interbeds and less-well-exposed laminated shales. These joints are often stained red along thin halos of several millimeters to a couple of centimeters thickness, and this staining is especially prominent near intrusions (Figs. 6D, 6E). We observed at least two joint sets at most intrusion locations, and their orientations are consistent throughout the study area (Figs. 7A, 7B). We contoured the unfolded joint orientations using a Kamb contour plot (Fig. 8A) and a 1% contour plot (Fig. 8B). The Kamb plot shows two systematic joint sets: a northwest-striking set and a northeast-striking set. The 1% contour plot shows a third less prominent joint set striking east-west that may not be statistically significant because they were found at only a few locations along the backlimb near the rabbit-ear structure and along the hinge of SMA. These joint orientations are consistent with joint sets reported in the Tensleep Sandstone and Amsden and Phosphoria Formations at SMA (Bellahsen et al., 2006). In these units, Bellahsen et al. (2006) found five systematic joint sets: set I was interpreted to predate Laramide compression and strikes 110°; set II was interpreted to be related to Laramide compression and strikes 45°; set III formed in response to the bending of layers and strikes 135°; set IV was interpreted to be related to late-stage fold growth and are vertical joints striking 110°; and set V comprises set I fractures that were reactivated as reverse faults in the forelimb during late-stage fold growth. The northeast-striking and northwest-striking joint sets reported here in the Mowry Formation are roughly parallel to sets II and III, respectfully, reported by Bellahsen et al. (2006). While we did not collect detailed data on abutting relationships (this is difficult to do with great confidence in the friable Mowry outcrops), based on the systematic nature of the joint orientations across the study area, it is plausible that the joints in our study area are temporally related to sets II and III of Bellahsen et al. (2006), although given the proliferation of the northwest-striking joints throughout our study area beyond the SMA fold hinge, the formation mechanism of the northwest-striking joints in the Mowry Formation is likely different than that of set III in the older units inferred by Bellahsen et al. (2006). The Peay Sandstone Member of the overlying Frontier Formation lacks any systematic joint sets in most locations in our study area.

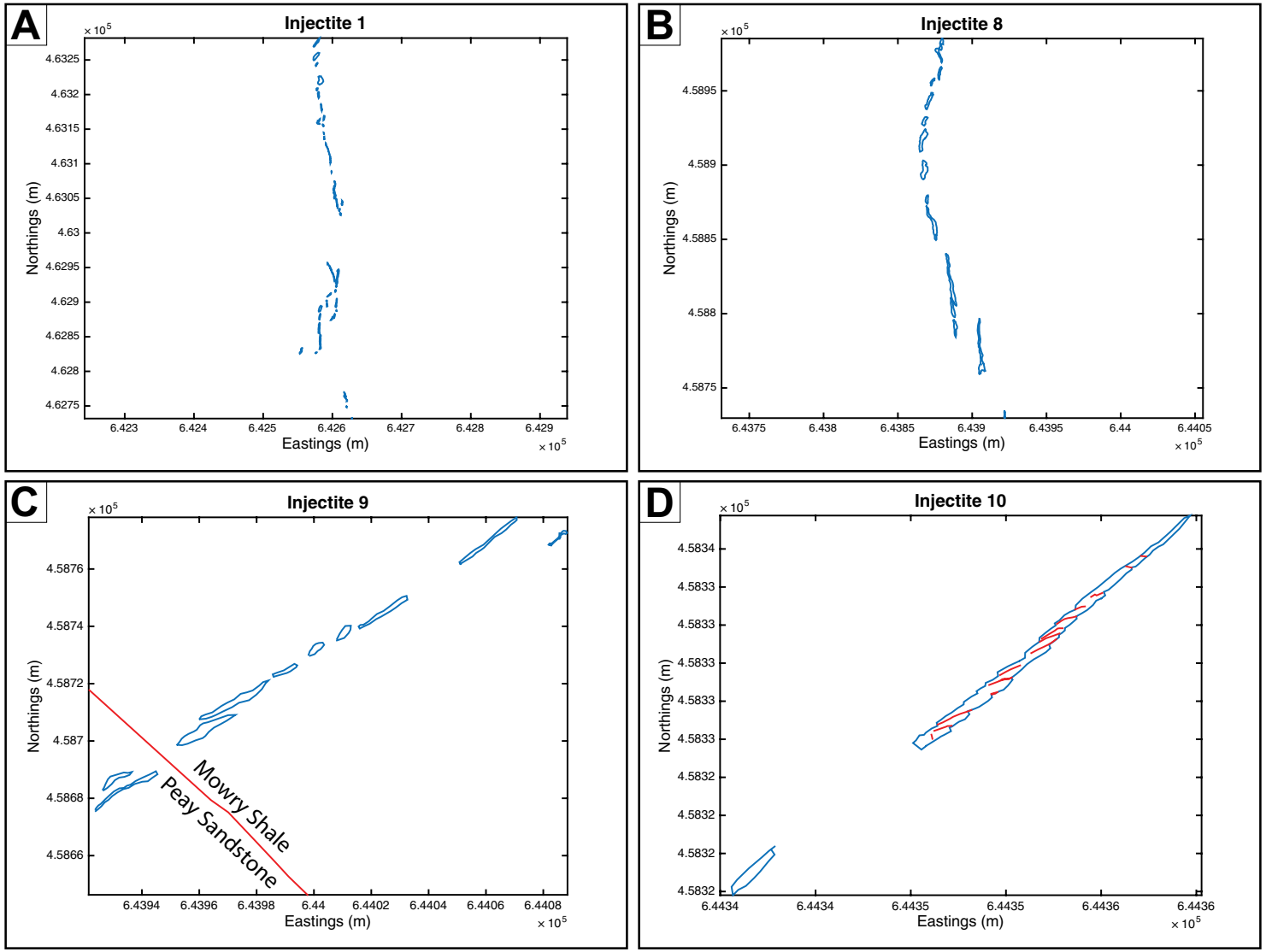

Figure 4. Two-dimensional plots of injectite contacts created in Matlab. (A) Injectite 1 extends for <1 km in outcrop length. (B) Injectite 8 shows evidence of mechanical interaction between the segments, where overlapping segments thin out at the tips. (C) Injectites crop out in the upper Mowry Formation and a few can be traced back to the Peay Sandstone Member. Injectite 9 extended a short distance above the base of the Peay Sandstone Member. (D) Injectite 10 is among the shortest in length, but could be traced back to the Peay Sandstone Member and pinched out at its lower extent. Throughgoing oblique normal faults (red) are parallel to deformation bands.

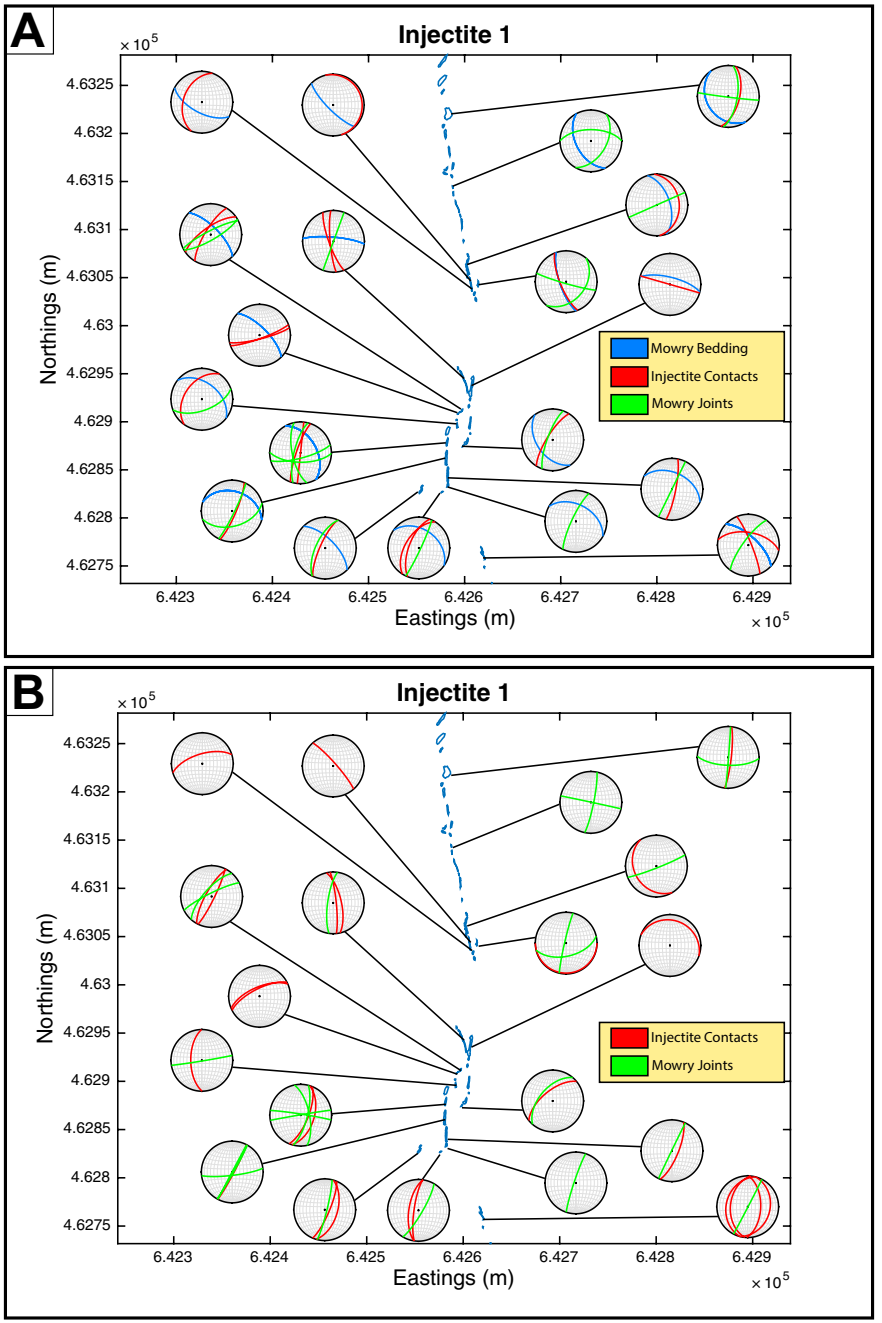

Figure 5. (A) Present-day orientations of Mowry bedding, Mowry joint sets, and injectite contacts for each segment of injectite 1. (B) Unfolded orientations of Mowry joints and injectite contacts for each segment of injectite 1. Most segments restore to subvertical, but a few restore to subhorizontal. For many segments, there is a joint set subparallel to the injectite contact.

Intrusion Material

The intrusion material is a buff-colored medium-grained sandstone. The framework grains of the sandstone contain ~70% quartz, 20% lithic fragments, 10% feldspar, and trace minerals. The sandstone is well sorted with subangular to subrounded grains ranging in size between 0.1 and 0.2 mm (Fig. 9A). Quartz grains are typically moderately fractured, particularly at grain contacts. This lithology is comparable to that of the Peay Sandstone Member of the Frontier Formation (Fig. 9B). Thin sections were also made of the Torchlight Sandstone Member of the Frontier Formation (Fig. 9C) and the Muddy Sandstone Member of the Thermopolis Shale (Fig. 9D), but neither was similar to the intrusion material in terms of lithology or porosity. While the overall compositions seem to be similar, the framework grains of the Torchlight Sandstone Member are more elongate (Fig. 9C), the Muddy Sandstone Member grains are slightly larger and more rounded (Fig. 9D), and porosity of the intrusion specimen is lower than in both of these units.

Deformation Bands

Most intrusion segments display two distinct sets of deformation bands, and in most locations the bands are mutually crosscutting, although in a few cases one set of deformation bands consistently offsets the other (Fig. 10B). In outcrop, deformation bands tend to form resistant ridges, and at the outcrop scale, deformation bands appear to range in thickness from 1 mm to 2 cm; however, closer inspection shows that individual bands are 1–2 mm thick (Fig. 10A) while thicker bands consist of zones of individual deformation bands (Fig. 10B), consistent with previous observations elsewhere (Aydin and Johnson, 1978). Described as zones of deformation bands (Aydin and Johnson, 1978) or compound deformation bands (Mair et al., 2002), these groups of adjacent deformation bands have total thicknesses of 1–2 cm (Fig. 10B). Aydin and Johnson (1978) interpreted compound deformation bands to represent a strain localization process, where initial deformation band formation produces a discontinuity favoring localization of subsequent bands. Compound bands, and less frequently individual deformation bands, also host slickensided fault surfaces (Fig. 10C), which form preferentially on the edge of preexisting bands. These surfaces have been interpreted as the last stage of deformation as faulting localized onto a single plane preferentially along the preexisting anisotropy introduced by the deformation bands (Aydin and Johnson, 1978). The faults in the intrusions at SMA are typically smaller in length than the intrusion width, and in rare cases cut through the entire intrusion. In the latter cases, the localized faults appear to transition into diffuse deformation in the Mowry Formation;

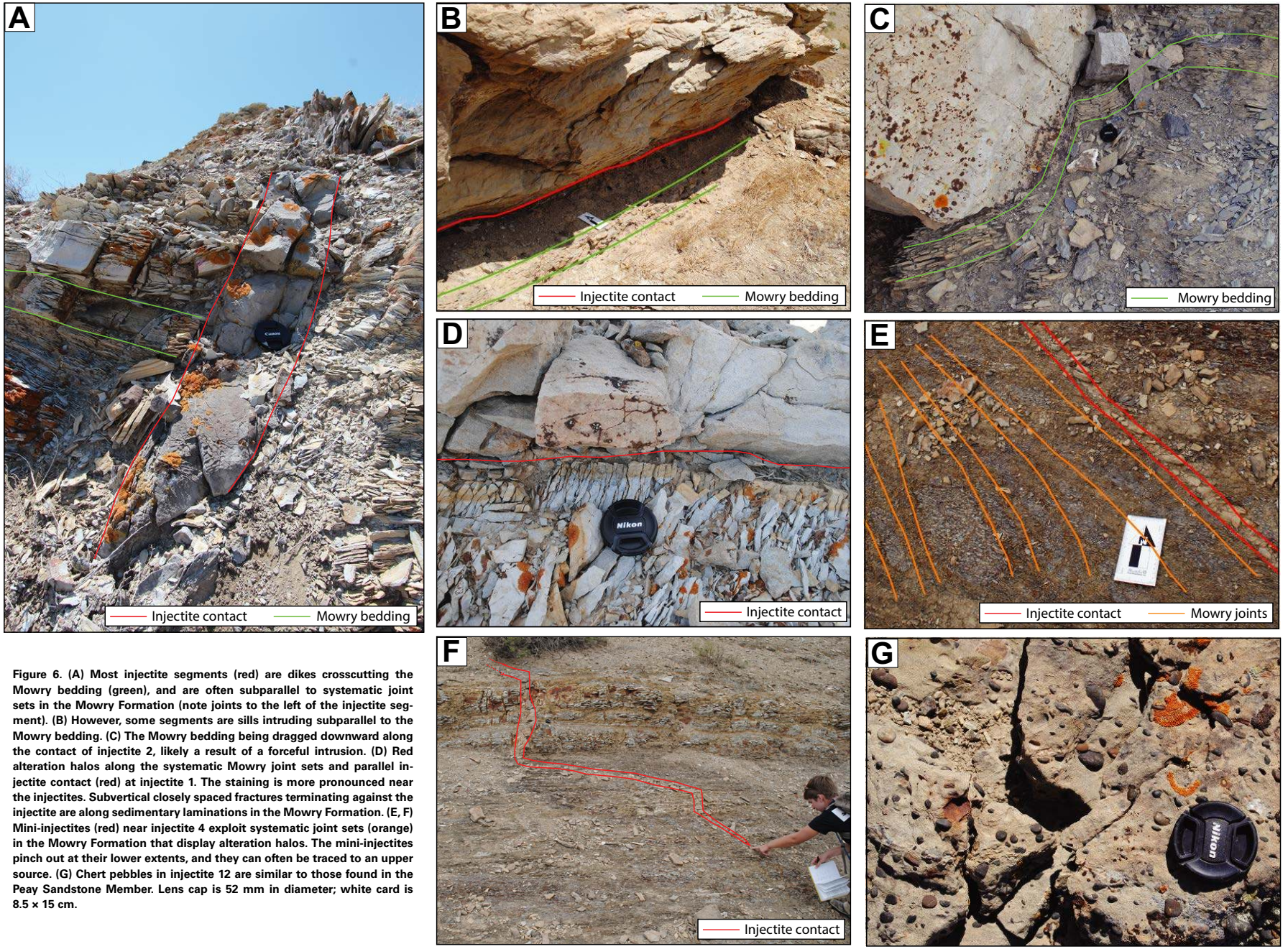

Figure 6. (A) Most injectite segments (red) are dikes crosscutting the Mowry bedding (green), and are often subparallel to systematic joint sets in the Mowry Formation (note joints to the left of the injectite segment). (B) However, some segments are sills intruding subparallel to the Mowry bedding. (C) The Mowry bedding being dragged downward along the contact of injectite 2, likely a result of a forceful intrusion. (D) Red alteration halos along the systematic Mowry joint sets and parallel injectite contact (red) at injectite 1. The staining is more pronounced near the injectites. Subvertical closely spaced fractures terminating against the injectite are along sedimentary laminations in the Mowry Formation. (E, F) Mini-injectites (red) near injectite 4 exploit systematic joint sets (orange) in the Mowry Formation that display alteration halos. The mini-injectites pinch out at their lower extents, and they can often be traced to an upper source. (G) Chert pebbles in injectite 12 are similar to those found in the Peay Sandstone Member. Lens cap is 52 mm in diameter; white card is 8.5 × 15 cm.

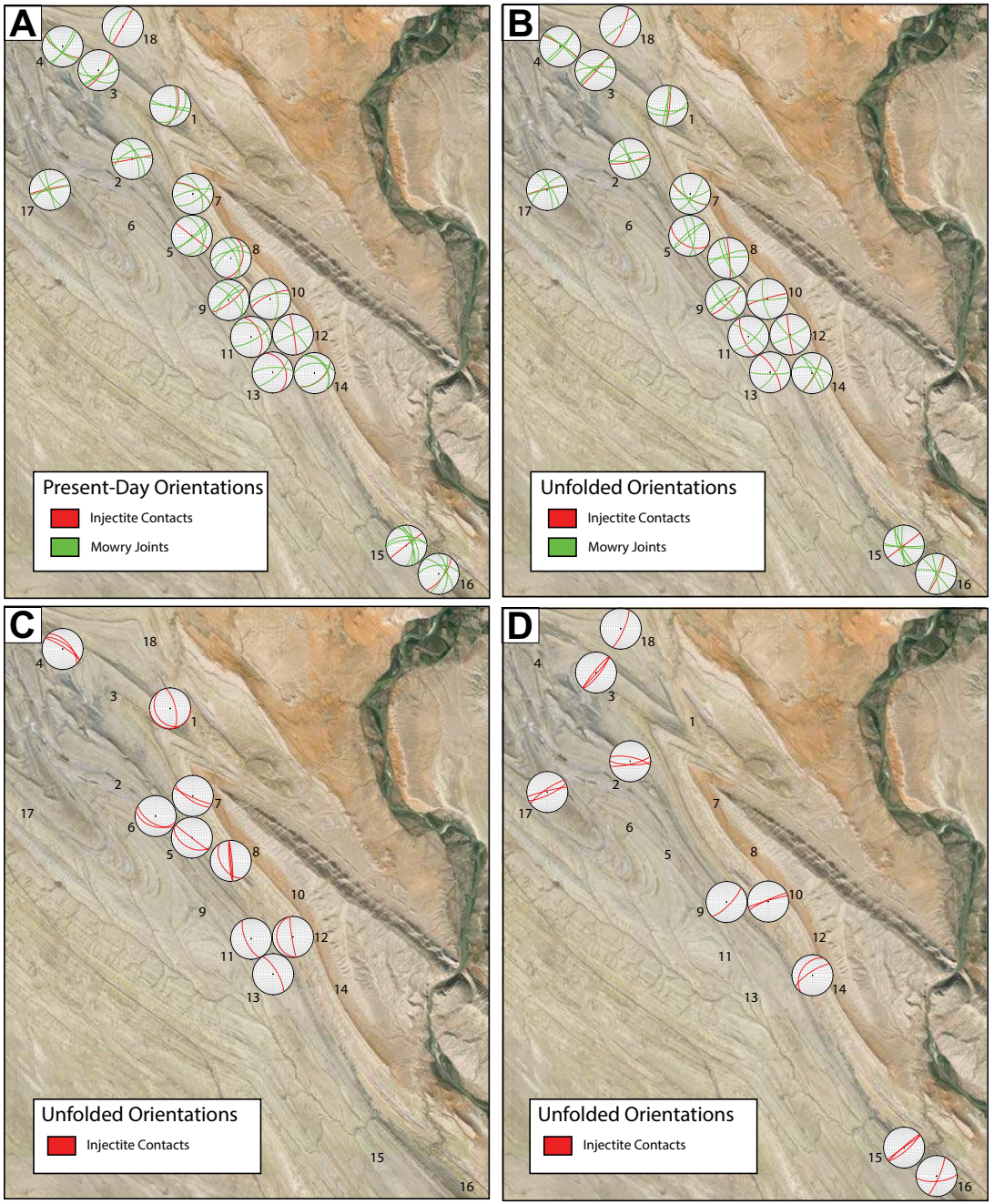

Figure 7. (A) Present-day orientations of injectite contacts and Mowry joints. (B) Unfolded injectite contacts and Mowry joints for each injectite. The contacts and joints were unfolded around the local Mowry bedding orientations. Based on their unfolded orientations, the injectites can be subdivided into two groups (C and D). (C) Northwest-striking injectites. (D) Northeast-striking injectites. There is no apparent relationship between the strike of the injectites and the location with respect to Sheep Mountain anticline. Note that in this figure injectite orientations are chosen as representative orientations, chosen as the average orientation among multiple (sometimes more than 20–30) individual segments (Fig. 5).

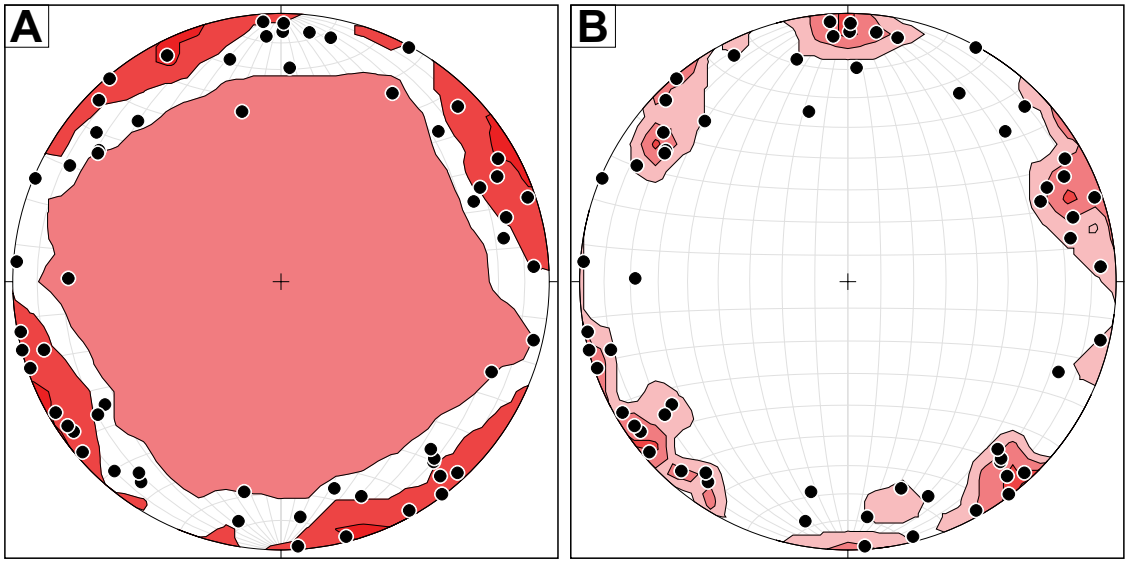

Figure 8. Contours of the poles to the unfolded Mowry joints in the study area. (A) Kamb contour plot showing two systematic joint sets in the Mowry Formation: a northwest-striking set and a northeast-striking set. (B) 1% contour plot showing three systematic joint sets in the Mowry Formation. In addition to the northwest-striking and northeast-striking sets found in the Kamb plot, the 1% contour plot recognized a less prominent set striking east-west.

however, poor outcrop quality made it impossible to characterize this deformation in detail. We were able to determine the sense of slip on a number of slickensided surfaces using crosscutting deformation bands as offset markers as well as steps in slickensides surfaces. Where possible, we used both criteria to insure a consistent interpretation. The majority of the deformation bands and slickensided surfaces exhibited reverse slip, whereas only a few indicated normal slip (Fig. 2A).

In thin section, the deformation bands are easily recognized by their significant loss of porosity (Fig. 11) and range in thickness from 0.2 mm to ~1.3 mm. The intrusions have ~15% porosity, but within the deformation bands porosity is <5%. Most deformation bands exhibit incipient cataclasis evident by microcracks growing from grain boundaries as well as minor pressure solution (Fig. 11A), consistent with the observations of Kunkle and Griffith (2011). In most samples, there is only a slight reduction in average grain size within the deformation bands, compared to grain sizes outside the deformation bands. A few deformation bands exhibit more significant deformation, evidenced by extreme comminution (Fig. 11B). These deformation bands also tend to be narrower than the deformation bands with very limited cataclasis.

The density of deformation bands varies between intrusions, and even between individual segments of a single intrusion. Some outcrops contain tens of bands per meter (Fig. 10A) and some contain hundreds of bands (Fig. 10B). While there is no clear pattern of deformation band density within a single intrusion, the deformation bands appear qualitatively to be better developed in the backlimb than around the nose of SMA.

At most intrusion locations, deformation bands are systematic at the outcrop scale and band orientation is consistent for each set across a single intrusion; however, deformation band orientation is less consistent from intrusion to intrusion in both the present-day and unfolded orientations (Figs. 12A, 12B). The deformation bands can be loosely subdivided into two generalized groups based on present-day orientations: a northeast-striking set (Fig. 12C) and a northwest-striking set (Fig. 12D).

Intrusion Direction Indicators

As described herein and in Figure 10, the Peay Sandstone Member is the only sandstone in the vicinity that has framework grains similar to those of the intrusion material (Warner, 1968). Furthermore, the intrusions locally contain abundant chert pebbles identical to those in the Peay Sandstone Member. In the field, intrusions 6, 9, 12, and 18 can be followed directly to the Peay Sandstone Member.

It has been argued that the intrusions at Sheep Mountain are of Neptunian origin (e.g., E. Erslev, 2014, personal commun.). The primary evidence to support this hypothesis is the inferred downward transport direction of the intrusive material that is in contrast to the forceful intrusion model discussed herein. The preferred downward intrusion direction at SMA is consistent with intrusions in glacial environments and Neptunian dikes; however, due to the inferred timing of intrusion, formation in a glacial environment can be ruled out (DeCelles, 2004; Fan and Dettman, 2009). Another key observation is that the intrusions are often subparallel to Mowry Formation joints (Figs. 6A, 7A, and 7B).

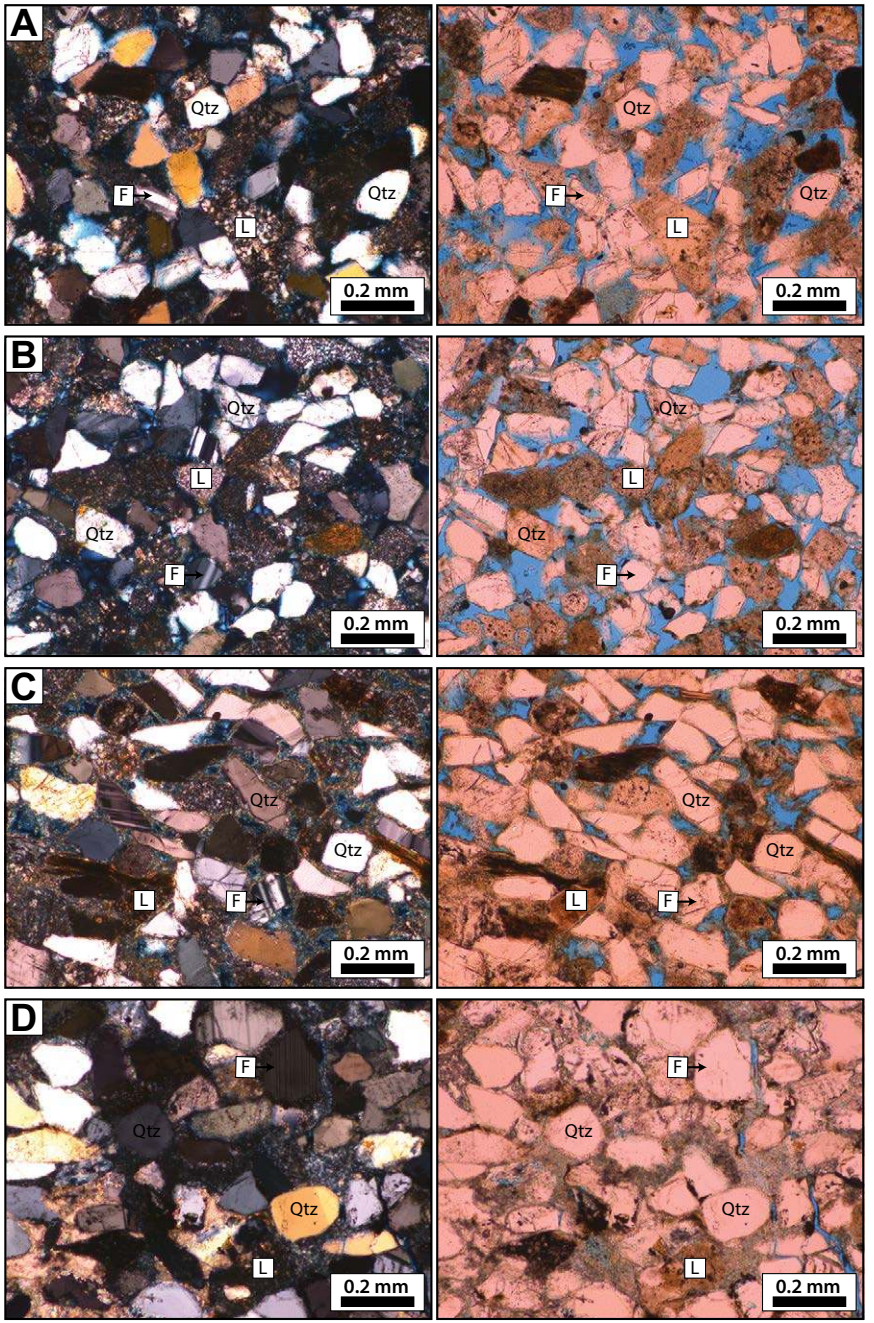

Figure 9. Photomicrographs of (A) injectite material; (B) the Peay Sandstone Member; (C) the Torchlight Sandstone Member; and (D) the Muddy Sandstone Member under cross-polarized light (left) and plane light (right). The injectite material and the Peay Sandstone Member are composed of ~70% quartz (Qtz), 20% lithic fragments (L), 10% feldspar (F), and trace minerals. Grain size and roundness is similar, with the injectite material being slightly more rounded. The Torchlight Sandstone Member has more elongated grains than the injectite material, while the Muddy Sandstone Member grains are more rounded and slightly larger. There is also significantly less porosity in the Muddy Sandstone Member.

When fractures form on the seafloor, they can be infilled by overlying sediments (Smart et al., 1988). Key characteristics of infilling would be horizontal layering, or vertical layering in the case that the fractures progressively widened, but these features may be absent if the fractures were rapidly infilled (Demoulin, 1978).

While a case can be made for a Neptunian origin for the intrusions at SMA, a number of field observations of wall-rock deformation consistently support the interpretation of a forceful intrusion. (1) At the intrusion contacts, the Mowry bedding is deformed. Adjacent to dikes, beds exhibit downward warping and drag folding (Fig. 6C), consistent with downward, pressurized sand transport. (2) While most intrusion segments restore to subvertical, several segments restore to subhorizontal, bedding-parallel sills. Sill formation requires supralithostatic pressure within the intrusive sands. (3) Mini-intrusions (<10 cm thick) have been documented at intrusions 4, 10, and 14. These mini-intrusions are always directed downward and pinch out at their lower tips (Fig. 6F), and they can usually be traced to an upper source. Mini-intrusions are parallel to joints along most of their length (Fig. 6E), occasionally cutting across, parallel to bedding, to adjacent joints (Fig. 6F). The mini-intrusions are always subparallel to and connected to larger intrusions, suggesting that they are small-scale representations of the larger scale intrusions. (4) Sandstone dikes (i.e., injectites that cut bedding at high angles) are often subparallel to at least one joint (Figs. 6A, 7A, and 7B). Along with the evidence presented by the mini-intrusions, this suggests that the sand intrusions may have at least partially exploited preexisting joints in many cases; however, at most locales intrusions also deviate from these orientations. While this observation could support the theory of Neptunian origin, suitably oriented joints could also be dilated if the pore fluid pressure within the intrusions exceeded the regional normal stress acting perpendicular to the joints (Delaney et al., 1986). The latter interpretation is supported by the spatial distribution of joints relative to dikes. Based on line surveys of joints in resistant sandstone beds with the upper Mowry at intrusion 1, the spatial density of systematic joints in the Mowry tends to increase as the distance to the intrusion decreases (Fig. 13). Delaney et al. (1986) made a similar observation along igneous dikes where there was a significantly greater dike-parallel joint density within 5 m of the dike contacts, and a decrease in joint density further beyond that; they interpreted the proximal increase in joint density as the process zone related to magmatic dike propagation. In contrast, passive infilling implies near-zero driving stresses, and by extension, near-zero stress intensity factor and the absence of a process zone (e.g., Delaney and

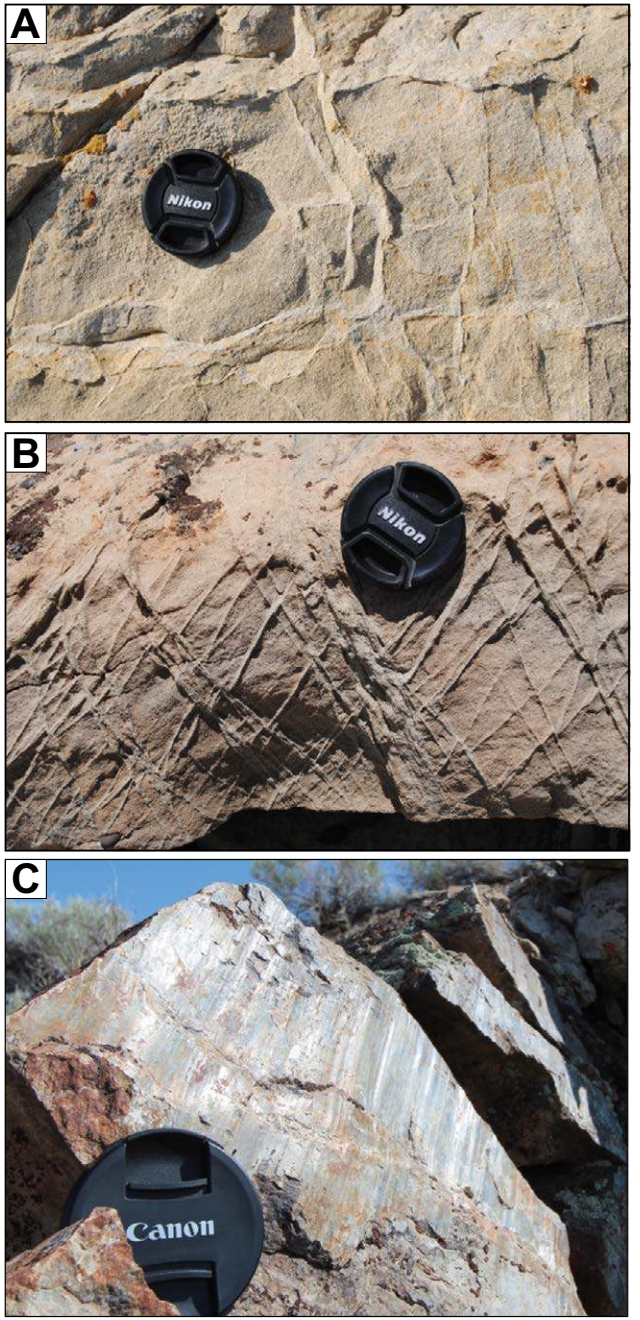

Figure 10. (A) Deformation is first accommodated in individual deformation bands. (B) As deformation progresses, compound deformation bands form as zones of deformation bands to accommodate displacement. (C) Eventually, deformation becomes localized onto a single plane, and a slip surface forms, accommodating much greater displacements. A and B also show the variation in density of deformation bands depending upon location. Lens cap is 52 mm in diameter.

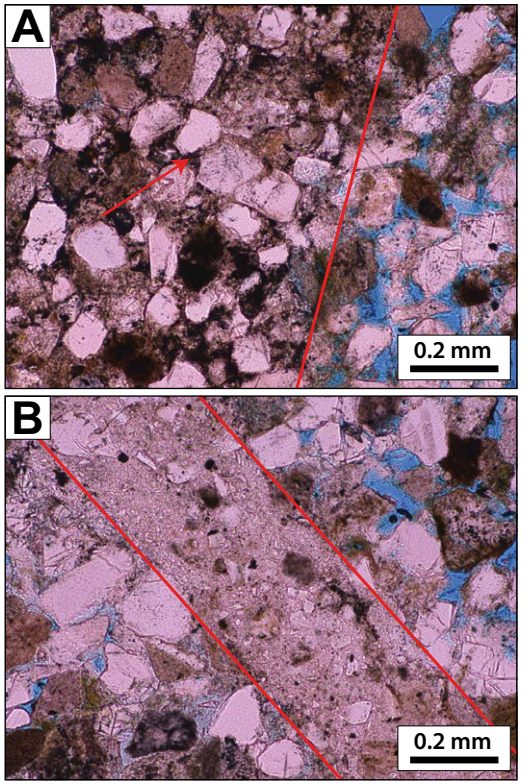

Figure 11. Photomicrographs of the deformation bands within the injectites under plane light. Both deformation bands are characterized by significant porosity loss. (A) There is only a slight reduction in grain size within the deformation bands, relative to the grain size just outside the deformation bands. Deformation mechanisms include cementation and minor pressure solution with concavo-convex contacts (red arrow). (B) A few deformation bands exhibit more advanced deformation, evidenced by extreme cataclasis. These deformation bands also tend to be narrower.

Pollard, 1981). (5) The segments of several injectites form an en echelon pattern (Figs. 2C and 4B), a pattern characteristic of mixed mode I–III fringes of otherwise opening mode fractures, including dikes, veins, and joints (Pollard and Aydin, 1988). While it is possible that such an arrangement of fractures could be formed initially, such as during lateral spreading within cohesive sediments of the upper Mowry Formation, and then passively infilled with sand, the fact that these fringes are found along the lateral and/or upper tips of injectites and infilled to such large aspect ratios suggests a forceful origin. Given the body of evidence for forceful intrusion of these intrusions, we prefer the injectite model for intrusion over passive infilling of sediments.

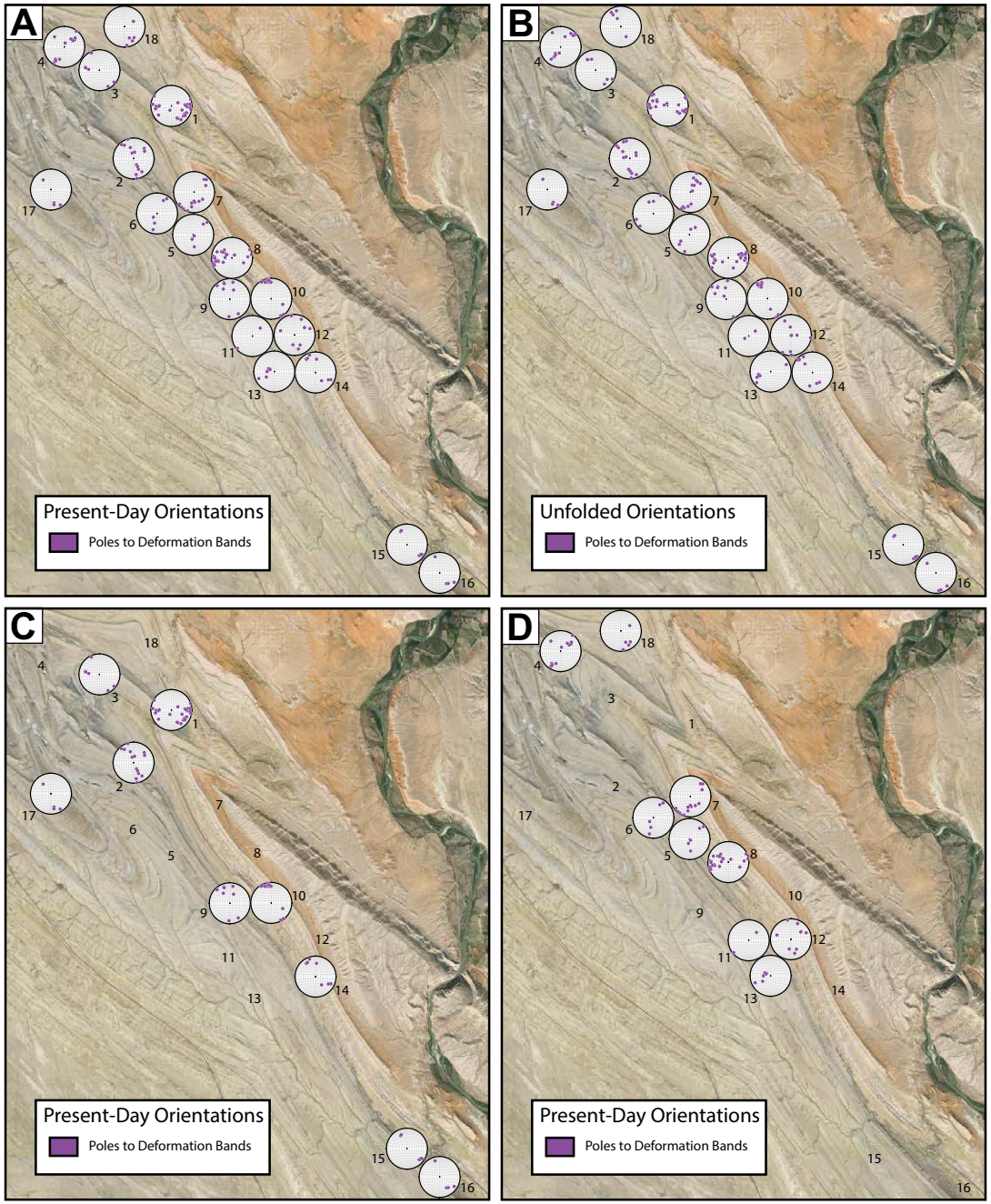

Figure 12. (A) Present-day orientations of deformation bands. (B) Unfolded orientations of deformation bands. Neither the present-day nor unfolded orientations of the deformation bands show a strong systematic relationship. However, using the present-day orientations, the deformation bands can be subdivided into two loosely defined groups (C and D). (C) Northeast-striking deformation bands. (D) Northwest-striking deformation bands.

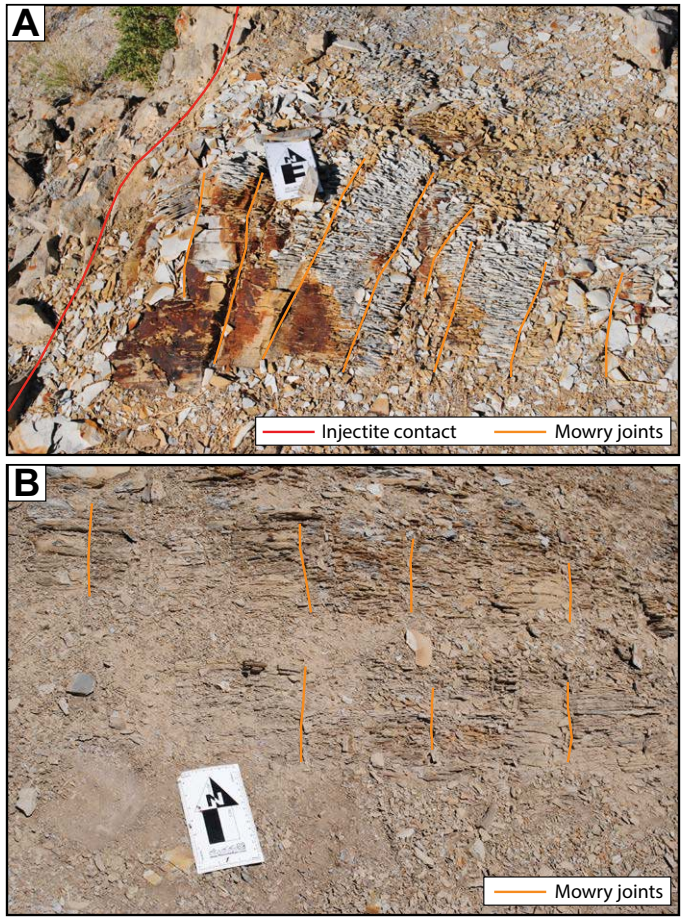

Figure 13. The spatial density of joints in the upper Mowry Formation increases as the distance to the injectites decreases. (A) Joint density near the contact at injectite 1 (left side of image). Close to the injectites, the joints are typically stained with alteration halos, presumably from hydrothermal fluids. (B) Further from the injectite contacts, the density of joints significantly decreases. White card is 8.5 × 15 cm.

DISCUSSION

Timing and Direction of Intrusion

Abundant data consistently suggest downward and lateral (in the third dimension) intrusion of the SMA injectites. Due to the subparallelism between injectites and local joint sets at some sites, and the lack of consistent abutting relationships, we must rely on complementary observations in order to determine the timing of jointing and sand intrusion. Unfolded injectite contacts (Fig. 5B) are either subvertical (dike) or subhorizontal (sill), suggesting that intrusion occurred prior to the folding of SMA, or during the early stages of folding, when the Mowry bedding was still nearly horizontal. Because the injectites appear to have, in many cases, exploited joint sets in the Mowry Formation, it is essential to determine the timing of formation for the Mowry joints. Based on no observed measurable shear displacement along the joints, we assume that they propagated as pure mode I fractures (i.e., in the σ_1-σ_2 plane). Although the northwest-southeast–striking set is similar in orientation to the set III fractures identified by Bellahsen et al. (2006), they likely did not form at the same time, or at least by the same mechanism, as the set III fractures, which were only found in the hinge of SMA. Amrouch et al. (2010) used calcite twins in the matrix of the Madison and Phosphoria Formations to interpret a prefolding maximum compressive stress oriented at 135°, subparallel to our northwest-southeast joints; two sites from their study also show microfaulting related to this compression trend. Amrouch et al. (2010) argued that the set I fractures identified by Bellahsen et al. (2006) (that range in strike between 110° and 140°) could be associated with this prefolding horizontal compression. Beaudoin et al. (2012) also interpreted a prefolding west-northwest–east-southeast compression from a combined analysis of fractures, fault-slip data, and calcite twinning. Therefore, we prefer an interpretation in which the northwest-southeast Mowry joints formed prior to Laramide contraction, when the greatest compressive horizontal stress has been interpreted to trend northwest-southeast (Bellahsen et al., 2006; Amrouch et al., 2010; Beaudoin et al., 2012). The northeast-southwest joint set is consistent with Laramide contraction (i.e., with greatest compressive horizontal stress northeast-southwest), similar to set II fractures reported by Bellahsen et al. (2006) in older units, and given that the unfolded orientations of northeast-southwest joints are markedly different than the present-day orientations, we interpret that they formed prior to or during the initial stages of folding.

Sorting out the timing of sand injection requires characterization of intrusion mechanics. As described previously, there is abundant evidence pointing to downward (and lateral) intrusion of the Sheep Mountain injectites. We first discuss a general model for downward intrusion of the sand injectites, and then utilize the 3-D geometry of the injectites to consider the overpressure gradients associated with injectite propagation. We integrate these results with structural orientation data collected in the field to produce a comprehensive model for sand injection at SMA.

Model for Downward Intrusion

The only well-known mechanism for downward intrusion of sandstone dikes is by flushing sediments into open fissures (Hurst and Cartwright, 2007), producing Neptunian dikes that typically range between 1 and 10 m in length (Talbot and von Brunn, 1989). These structures usually display horizontal layering suggesting progressive infillings, or vertical layering suggesting multiple

infillings as the fractures widened over time (Demoulin, 1978). This method of intrusion does not seem likely based on the evidence described herein, and also because the injectites can be as long as 1 km, much larger than any other Neptunian dike occurrences we have found in the literature. Given this interpretation, and in light of the general model for forceful upward intrusion (Jolly and Lonergan, 2002), we describe an alternative mechanism in the following.

Simonson et al. (1978) showed that for vertical hydraulic fractures, stress gradients and heterogeneous material properties of the country rock play a major role in the fracture propagation. For example, for a vertical hydraulic fracture in an otherwise homogeneous medium, if the vertical pressure gradient within the fracture is greater than the gradient of the normal stress resisting injectite opening, the stress intensity factor of the lower tip exceeds that of the upper tip, making downward propagation probable (Simonson et al., 1978). We explore this possibility for the SMA injectites in the following section. Furthermore, in sedimentary rocks, variations in the in situ stresses arise during burial due to different material properties, as well as burial, lithification, and diagenetic histories. As a result, horizontal normal stresses can also be highly stratified, raising the possibility that the local confining pressures may be locally smaller in rocks underlying the sand layer than they are in the rocks above (e.g., Bourne, 2003; Simonson et al., 1978). In the case of the Sheep Mountain injectites, the sand was injected into a shale unit with interbedded sandstone layers, and at most localities, they were contained by the downward transition into a pure shale unit. Here, we explore the potential influence of heterogeneous material properties on the local stress field by considering potential effective elastic properties of each of these rock or sediment layers.

To do this, we take into account, in an approximate sense, the depositional, burial, and lithification history of the rock units involved in sand injection. For illustrative purposes, we neglect thermal and chemical contributions to stress changes. At the time of intrusion, the Peay Sandstone Member was a saturated sand, not yet lithified, on top of the previously fractured Mowry Formation (which may or may not have been completely lithified) and sealed from above by the bentonite-rich middle member of the Frontier Formation. The change in horizontal normal stress within each of the stratigraphic layers with burial depends on the degree of lithification and material properties of each layer (Maltman, 1994). The horizontal normal stress is also dependent upon the coupling between adjacent layers (Bourne and Willemse, 2001); however, by analyzing the evolution of stresses in each layer individually, we can ignore this coupling. In general, the change in the horizontal least compressive stress σ_h can be related to a change in vertical lithostatic stress σ_v by a ratio K by the relationship

$$\sigma_h = K\sigma_v. \quad (1)$$

For well-lithified rocks idealized as elastic materials in a basin under a state of uniaxial strain, K is a function of Poisson's ratio (ν):

$$K = \frac{\nu}{1-\nu}. \quad (2)$$

It should be noted that this assumption is a gross approximation given that the Mowry Formation contains systematic vertical joints, evidence of an anisotropic stress field prior to injectite formation; however, an anisotropic horizontal stress field does not invalidate the implied mechanism explained herein. For sediments, K is determined in the laboratory using triaxial compression experiments (Maltman, 1994). Based on the typical range for Poisson's ratio (Gercek, 2007), K typically varies between 0.15 and 0.53 for rocks, with sandstone and shale having approximate K values of 0.25 and 0.45, respectively, and based on experimental data, K varies between 0.3 and 0.7 for sediments (Maltman, 1994). The least compressive principal stress can be modeled as a function of the lithostatic stress and K. For sedimentary rocks K is also a function of time, decreasing as the sediments undergo compaction and lithification. Therefore, an accurate estimate of the horizontal stress in any unit involved needs to take into account the depth at which a unit lithified. To illustrate how the burial history of the sedimentary rocks involved in the SMA injectites may have resulted in downward injection of the Peay sand, we assume a lithification depth of 350 m for both the upper and lower Mowry Formation to develop plots of the evolution of σ_h. For the Peay unit and the overlying mud unit, we assume they were still unlithified at the time of the intrusion, and therefore, σ_h in these layers only depended on one K value.

Figure 14 is a model for injectite intrusion modified from the general intrusion model (Jolly and Lonergan, 2002). It follows from the previous discussion that before the sand body becomes sealed, the pore fluid pressure increases along the hydrostatic gradient. When the sand body becomes sealed, the pore fluid pressure will divert from the hydrostatic gradient along the lithostatic gradient, and intrusion commences once the pore fluid pressure exceeds the confining pressure. By including the effects of mechanical stratigraphy even in an approximate sense, it is possible to produce a scenario wherein the confining pressure in the shale unit below the sand body is smaller than in the mud unit above the sand body. This scenario would promote downward intrusion of the sand. This same concept could also be used to explain why we do not find the injectites in the lower Mowry Formation. The interbedded sand layers in the upper Mowry, as well as the preexisting joints that formed in response to a compressive horizontal stress, may have played a role in promoting fracture propagation while the lack of sand layers in the lower Mowry, resulting in a greater local σ_h, may have acted as a barrier to propagation.

Overpressures Driving Sand Injection

According to linear elastic fracture mechanics (LEFM), mode I fracture propagation occurs when $K_I = K_{IC}$, where K_I is the crack tip stress intensity factor and K_{IC} is the fracture toughness of the material (Rubin, 1993). For simple LEFM cracks with a uniform stress drop and homogeneous material properties, this criterion is straightforward to evaluate (e.g., Tada et al., 1985). However, for fluid-filled cracks, these conditions are often not met (Rubin, 1995). This may be due to varying material properties, a stratified remote stress field, two-phase flow within the injectites, and/or bleeding of fluid into the wall rock during propa-

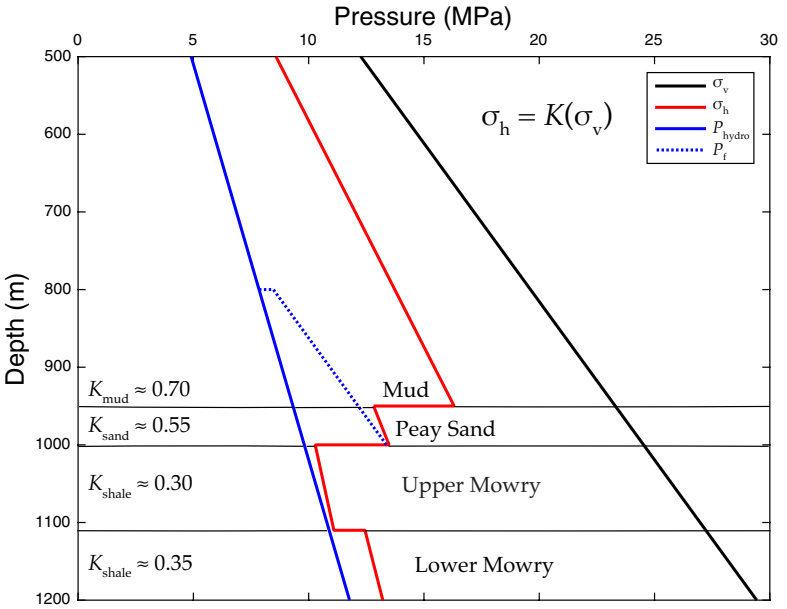

Figure 14. Model for downward intrusion modified from the Jolly and Lonergan (2002) model for upward intrusion. By considering the lithification history of the units involved, the confining pressure is dependent upon the elastic properties of the rocks. Here, we assume the Peay sand unit and the overlying mud unit were still unlithified at the time of intrusion. With this it is possible to have a scenario where the confining pressure below the sand body is smaller, allowing for downward intrusion. *K* values (Equation 1) are defined for each unit. Peay sand—Peay Sandstone Member.

gation. The net effect of these features can be incorporated into LEFM crack models by superimposing several simple contributions to crack face tractions (Delaney and Pollard, 1981; Bürgmann et al., 1994; Willemse and Pollard, 1998).

We modeled the injectites at SMA as single-segment pressurized cracks following the approach outlined by Delaney and Pollard (1981). Because the lateral length of the injectites is much greater than the vertical height (Table 1), we idealize the injectites as vertical, blade-like cracks (Fig. 15A), an assumption that allows us to model them assuming 2-D plane strain. Using the vector position data obtained while mapping the injectites, the apertures for each injectite were plotted as a function of elevation (Fig. 15C). If the blade-like dike geometry is valid, then variations in the lateral positions of the dike thickness measurements (along the x-axis) should not introduce appreciable error in the simplified vertical aperture distribution (Fig. 15A). We considered three simple contributions to crack loading (Fig. 15B), for which analytical solutions are available: a uniform normal stress, a linear normal stress gradient resulting in a symmetrical stress distribution, and a linear normal stress gradient resulting in an asymmetric stress distribution (solutions obtained from Delaney and Pollard, 1981; Lachenbruch, 1961; Pollard and Muller, 1976, respectively).

For a vertical 2-D dike with half-length a, position along the dike z, and aperture v_0, we can define the dimensionless variables $Z = z/a$ and $D(Z) = v_0/a$, where Z and D are dimensionless height and aperture of the dike, and v_0 and a are the aperture and half-height, respectively (Fig. 14B).

In this coordinate system, the origin is fixed at the center of the injectite, and the positive z direction is up (Fig. 15B). The opening distribution along the crack can be written as:

$$D(Z) = C_1F_1(Z) + C_2F_2(Z) + C_3F_3(Z), \quad (3)$$

where

$$F_1(Z) = (1 - Z^2)^{1/2} \quad (4)$$

$$F_2(Z) = \{(1 - Z^2)^{1/2} + Z^2 \ln|Z/[1 - (1 - Z^2)^{1/2}]|\} \quad (5)$$

$$F_3(Z) = Z(1 - Z^2)^{1/2}, \quad (6)$$

and

$$C_1 = S_0(1 - \nu)/\mu \quad (7)$$

$$C_2 = S_s a(1 - \nu)/\pi\mu \quad (8)$$

$$C_3 = S_a a(1 - \nu)/2\mu. \quad (9)$$

TABLE 1. AVERAGE ORIENTATION, HEIGHT, MAXIMUM APERTURE, AND CONSTANTS FOR EACH INJECTITE EVALUATED

Injectite	Average injectite strike (°)	Height (m)	Length (m)	Maximum aperture (m)	C_1	C_2	C_3
3	N35E	58.3	234.7	1.66	–0.0018 ± 0.0046	0.1004 ± 0.0035	0.0584 ± 0.002
8	N05W	142.9	217.3	2.7	0.0193 ± 0.0003	–0.0037 ± 0.0002	0.0064 ± 0.0002
9	N53E	82.2	175.7	2.71	0.0112 ± 0.0016	0.0125 ± 0.0011	0.0201 ± 0.0006
10	N60E	7.7	31.1	0.44	–0.0369 ± 0.0037	0.0796 ± 0.003	0.0013 ± 0.0018
15	N50E	10.3	30.4	0.87	0.0228 ± 0.0039	0.0882 ± 0.0029	0.0128 ± 0.0015
17	N71E	30.0	220.2	2.54	–0.0093 ± 0.0029	0.0441 ± 0.0023	0.0084 ± 0.0012

Note: C_1, C_2, and C_3 are constants that determine the relative importance of the overpressure distribution terms S_0, S_s, and S_a. Constants are reported with 95% confidence intervals.

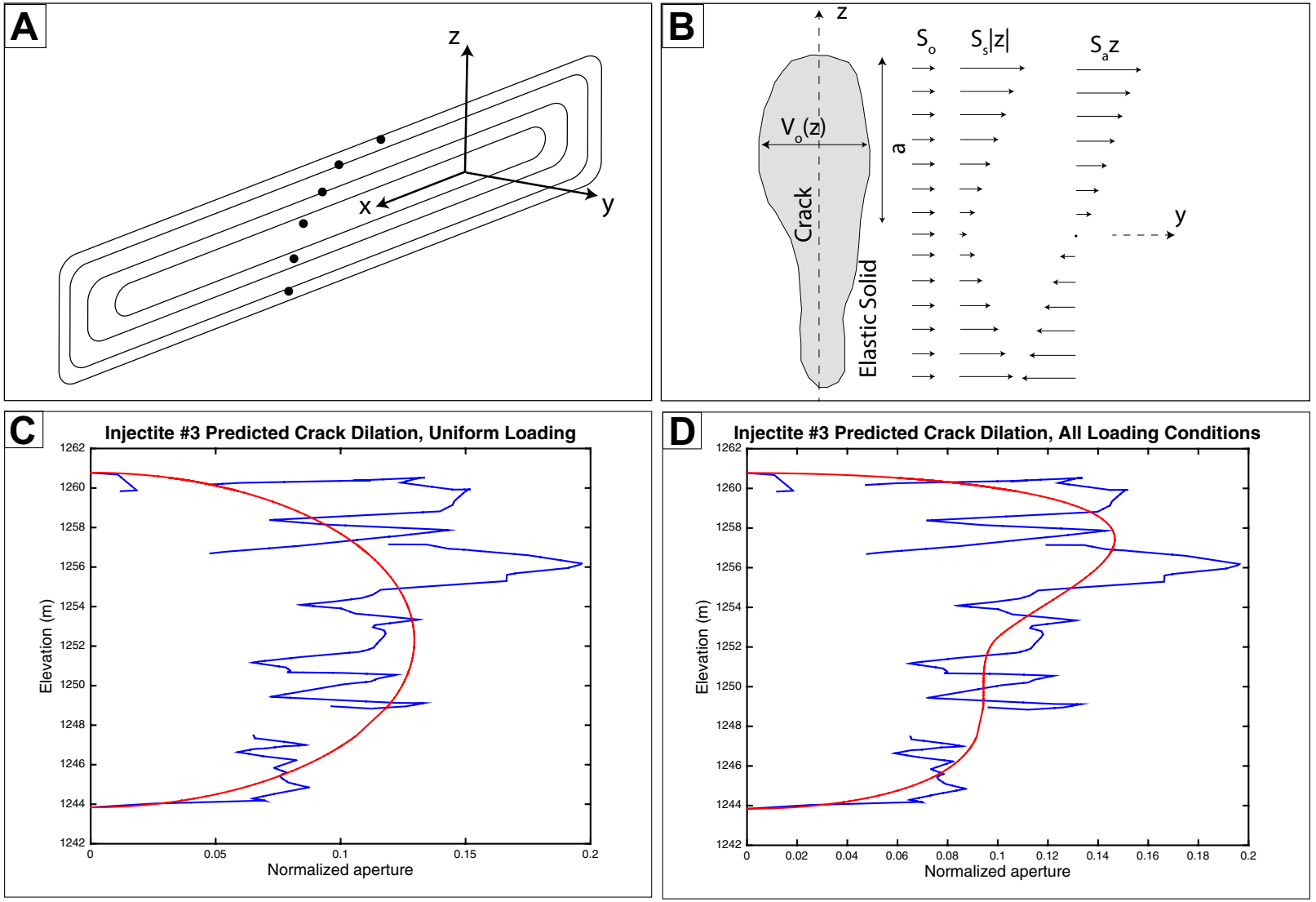

Figure 15. (A) The injectites are idealized as blade-like cracks, with the lateral length being much greater than the vertical length. (B) Cross section of a crack subjected to uniform normal stress (S_o), symmetrical linear stress gradient ($S_s|Z|$), and asymmetrical linear stress gradient (S_aZ) (modified from Delaney and Pollard, 1981). (C) Measured apertures (blue) and predicted crack dilation for injectite 3 under uniform loading. (D) Measured apertures (blue) and predicted crack dilation for injectite 3 as a function of the uniform, symmetric, and asymmetric loading conditions, which better approximates the opening distribution along the injectites.

In these equations S_0, S_s, and S_a are the uniform, linear symmetric, and linear asymmetric overpressure distributions, respectively (Fig. 15B). The total pressure distribution is a sum of the three loading conditions, such that:

$$S(Z) = S_0 + S_s a|Z| + S_a aZ. \quad (10)$$

It is important to note that we invert for the constants C_1, C_2, and C_3, not S_0, S_s, and S_a. The elastic compliance represented by $\frac{(1-\nu)}{\mu}$ is also unknown; therefore it is impossible to calculate the in situ stress gradients exactly as the variations in C_1, C_2, and C_3 can be partially explained by variations in compliance as a function of distance along the crack (e.g., Bürgmann et al., 1994; Rowe et al., 2012; Griffith et al., 2012). The exact magnitudes of the calculated overpressure gradients are less important than the general trends in the gradients, given the lack of constraints on rock properties in situ at the time of intrusion, although in the following discussion we substitute representative compliance values to illustrate the physical meaning of the results. We determined the relative contribution of each loading condition (coefficients C_1, C_2, and C_3; Table 1) to the total overpressure distribution within the injectites using the multiple-linear regression model:

$$T_i(Z) = C_1F_1(Z) + C_2F_2(Z) + C_3F_3(Z) + d_i, \quad (11)$$

where T_i is the dike aperture measured in the field, and d_i is the residual between the measured and calculated aperture at each height, Z. The predicted dilation calculated as a function of the three loading conditions (Fig. 15D) better predicts the opening distribution than when calculated from only the uniform loading condition (Fig. 15C) (i.e., only including the first term in Equation 11), indicating that the vertical pressure distributions were likely nonuniform. The pressure profiles were calculated for 6 of the 18 injectites, chosen based on the quality of outcrop data and the simplicity of the geometry. In some cases injectites were deformed during folding to the point that constraining their initial geometry is not possible.

The constant C_1 can be negative or positive, while the constants C_2 and C_3 are positive (Table 1). Because C_1 and C_2 are symmetric terms, and C_3 is positive, if we assume that material compliance is constant over the length of the injectites, this implies that the driving stress (fluid overpressure) is largest near the top of the injectite; however, because C_2 is nonzero, this gradient is not constant. Given the heterogeneity of the upper Mowry Formation, the assumption of uniform material compliance is probably unreasonable. Therefore, although part of this trend is likely due to the actual fluid overpressures in the dike, some may be due to variations in effective elastic properties, cohesion, or inelastic deformation along the fault, all of which may play a role in variations in crack face tractions (e.g., Bürgmann et al., 1994; Martel, 1997; Willemse and Pollard, 1998).

For illustrative purposes, in the subsequent analysis we choose uniform representative values for the compliance ($\nu = 0.25$ and $\mu = 40$ MPa, representative values for semiconsolidated sandy clay; Bowles, 1996) to obtain stresses and stress gradients (Table 2). The best-fit pressure profile is similar in form for every injectite, with the linear asymmetric gradient decreasing with depth in each case. The total overpressure, summing over all terms, is greatest at the top of the injectites. For shorter injectites, the symmetric gradients are much larger than the asymmetric gradients, although variance in the absolute value of stresses could easily be explained in terms of variability in material properties.

Results of stress intensity factor calculations are remarkable in several respects (Table 2). First, the large values of the stress intensities at both tips are the result of local overpressure maxima occurring near the tips. If the injectites simply exploited preexisting joints, as would be the case for the Neptunian dike scenario, we would expect near-zero stress intensities near the injectite tips, consistent with having an opening distribution that asymptotically approaches zero near the crack tips, similar to the bell-curve displacement distribution that results from cohesive end-zone models of fractures (Barenblatt, 1962; Willemse and Pollard, 1998). What we observe instead are blunt ends to the opening distributions (Figs. 15C, 15D), consistent with stress intensity factors larger than those predicted by the simple uniform loading case. In the field,

TABLE 2. IMPLIED PRESSURE COEFFICIENTS ASSOCIATED WITH INJECTITES IN TABLE 1, AND STRESS INTENSITY FACTORS FOR THE UPPER AND LOWER INJECTITE TIPS

Injectite	Height (m)	Length (m)	Maximum aperture (m)	S_o (MPa)	S_s (MPa m^{-1})	S_a (MPa m^{-1})	K_I^{top} (Mpa m$^{1/2}$)	K_I^{bottom} (Mpa m$^{1/2}$)
3	58.3	234.7	1.66	–0.0955 ± 0.2452	1.9873 ± 0.0692	0.7560 ± 0.0249	39.9603 ± 2.1049	21.8269 ± 1.4922
8	142.9	217.3	2.7	1.0333 ± 0.0163	–0.0086 ± 0.0006	0.0097 ± 0.0002	8.3022 ± 0.4238	2.5119 ± 0.2880
9	82.2	175.7	2.71	0.5977 ± 0.0812	0.0524 ± 0.0047	0.0537 ± 0.0016	19.0491 ± 1.4839	5.4417 ± 1.0661
10	7.7	31.1	0.44	–1.973 ± 0.1979	3.488 ± 0.1334	–0.0362 ± 0.0507	12.62 ± 1.2125	12.89 ± 0.8328
15	10.3	30.4	0.87	1.2186 ± 0.2381	2.8826 ± 0.1101	0.2663 ± 0.0362	25.5892 ± 1.5621	22.5004 ± 1.1419
17	30	220.2	2.54	–0.4985 ± 0.1565	0.5038 ± 0.0262	0.0610 ± 0.0085	17.8738 ± 1.7785	14.4373 ± 1.2995

Note: S_o, S_s, and S_a are the uniform, linear symmetric, and linear asymmetric overpressure distributions, respectively; K_I^{top} and K_I^{bottom} are the calculated stress intensity factors for the upper and lower injectite tips, respectively. All terms are reported with 95% confidence intervals.

injectite segments can be found exploiting joints and bedding discontinuities, but otherwise crosscutting bedding layers. Therefore we conclude that the injectites either forcefully connected previously discontinuous joints confined to individual mechanical layers within the Mowry Formation, or they formed at the same time as the joints, contrary to previous interpretations (Warner, 1968). The latter interpretation provides a simpler explanation for why injectites follow both joint sets at different locations around SMA, and supports our earlier hypothesis that the northwest-striking injectites formed prior to folding when the maximum horizontal stress was oriented northwest-southeast, and the northeast-striking injectites formed during the early stages of folding when the maximum horizontal stress was oriented northeast-southwest. Note that our calculated stress intensity factors are an order of magnitude larger than laboratory estimates of the fracture toughness of common rocks (Atkinson and Meredith, 1987), consistent with previous field estimates of the stress intensities associated with magmatic dikes (Delaney and Pollard, 1981). Based on the well-known proportionality between the stress intensity factor and the energy release rate (e.g., Irwin, 1958), this discrepancy could be explained by the energy consumed in production of joints in the process zone around the injectite tip (Delaney and Pollard, 1981; Delaney et al., 1986). This interpretation is consistent with our observation of local increases in joint density proximal to injectites (Fig. 13A). The calculated stress intensity factor is always greatest at the upper tip of the injectite, although the values calculated for the upper and lower tips are similar in several cases. This seems inconsistent with downward propagation; however, it is consistent with why downward propagation was terminated. Presumably the injectites propagated until the lower stress intensity factor was below the fracture toughness of the Mowry layering; therefore, it is possible that during downward injectite propagation, the stress intensity factor at the lower tip was higher (and, by extension, the fluid pressure gradient exceeded the confining pressure gradient).

Timing of Deformation: A Comprehensive Model of Sand Injection at SMA

The deformation bands are contained within the injectites; therefore, they likely formed after injectite intrusion and lithification. Neither the current attitudes nor the unfolded attitudes of the deformation bands show any obvious systematic relationships, spatial or temporal. However, they may be related by common principal deformation axes. To check for kinematic compatibility of the deformation bands, we performed a Bingham analysis (Marrett and Allmendinger, 1990) on both the present-day and unfolded deformation band orientations. This graphical method uses the orientation of the fault plane, slip direction, and the sense of slip to determine the shortening and extension axes for each fault surface.

We determined the sense of slip for 15 of the 18 injectites; 9 of the 15 exhibited reverse slip on the slickensided surfaces. After the analysis, these injectites showed subvertical extension axes and northeast-southwest shortening axes (Fig. 16A), which were consistent along the length of each injectite. This northeast-southwest shortening is in agreement with the paleostress regime associated with set II fractures of Bellahsen et al. (2006), as well as that inferred from calcite twins in the Madison and Phosphoria Formations and the Tensleep Sandstone (Amrouch et al., 2010). These axes suggest deformation band formation during Laramide contraction and the folding of SMA. During the late Pliocene and early Pleistocene, regional uplift of mountain ranges caused extensional faulting in the basins (Love, 1960; Ray and Keefer, 1985; Byrd et al., 1994; McMillan et al., 2006). Amrouch et al. (2010) inferred a post-folding northeast-southwest extension from calcite veins in sets I and III fractures and hypothesized that this recorded extension may indicate outer rim extension; however, they could not rule out the possibility that the extension was linked to the permutation of set I principal axes. Beaudoin et al. (2012) obtained paleostress tensors from calcite twinning at Rattlesnake Mountain anticline, west of SMA; they found indicators of an east-west extension that clearly postdated Laramide compression. This extension event was tentatively related to Basin and Range extension. There is a general agreement that the Bighorn Basin underwent post-folding extension, although the direction of extension varies from study to study. We identified normal slip on the slickensided fault surfaces of six injectites at SMA. The kinematic analysis showed that these six injectites underwent northwest-southeast horizontal extension (Fig. 16B), subparallel to the axial trace of SMA; this is consistent with deformation band formation occurring after the Laramide orogeny, during post-folding extension.

CONCLUSIONS

Sandstone injectites are common features in sedimentary environments around the world; however, in most cases they are not easily accessible, and therefore are difficult to study at subseismic resolution. SMA offers unique exposures of sandstone injectites that have been subsequently deformed. We characterized injectites at SMA located around the nose and west flank of the fold. The injectites formed during the early stages of folding of SMA. They were deformed during Laramide orogenic contraction and the formation of SMA, but upon unfolding around the local bedding orientations, the injectites restore to dike and sill orientations. These injectites were sourced from the Peay Sandstone Member of the Frontier Formation and propagated downward and laterally into the Mowry Formation in orientations consistent with the two major joint sets found throughout the field area. Sand injection was driven by overpressurized pore fluids in the Peay Sandstone Member and a stratified σ_h, which arose from the depositional, burial, and lithification history of the rock units. Injectites show evidence of interaction between individual injectite segments and joints in the Mowry Formation, and although it is unclear based on simple field relationships whether the joints formed before, or simultaneously with, sand injection, joint spacing decreases near the injectites, suggesting forceful intrusion and damage of wall rocks during dike propagation. Our calculations of overpressure profiles and stress intensity factors associated with several injectites are consistent with intrusion

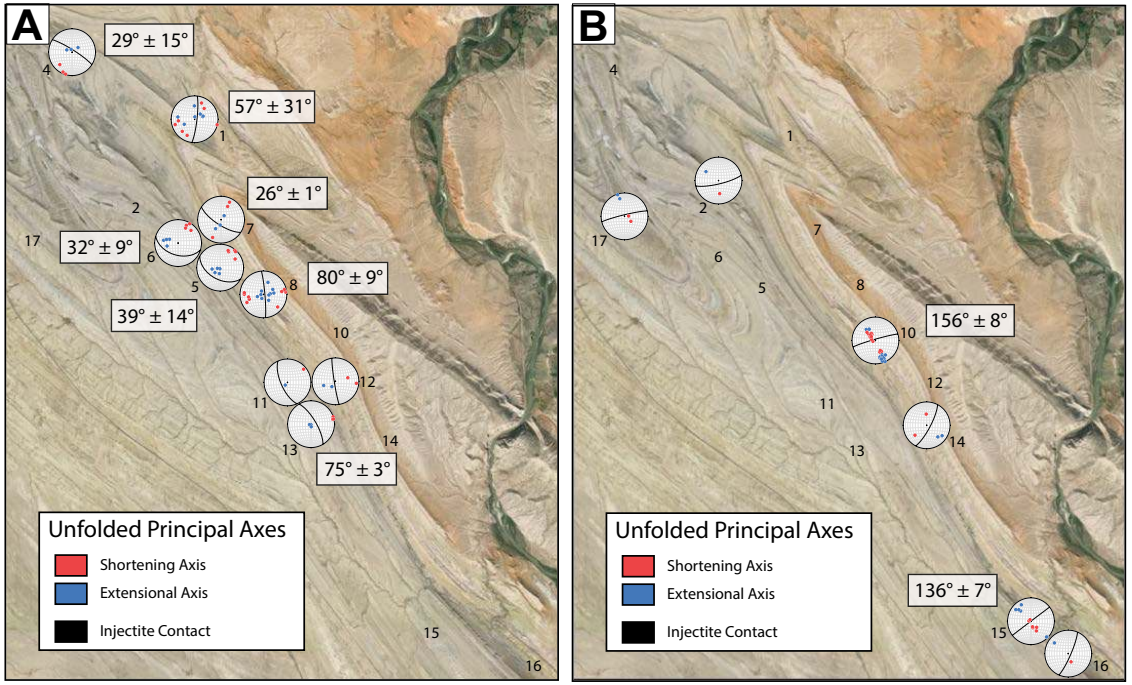

Figure 16. Unfolded principal axes of deformation for the deformation bands. (A) Some of the injectites contained deformation bands that exhibited reverse slip, consistent with Laramide contraction. (B) Some injectites contained deformation bands that exhibited normal slip, consistent with post-folding extension. Mean shortening and extensional directions are recorded for sites with adequate data in A and B, respectively.

of intact rock or cohesive sediments; therefore we prefer the interpretation that injectites formed at the same time as joints. Subsequent deformation resulted in the formation of deformation bands, which form the dominant internal fabric of the injectites. These deformation structures formed after sand intrusion and were subsequently faulted, resulting in slickensided surfaces. While there is no observable trend in the attitude of the deformation bands, common principal axes of deformation were obtained from a kinematic analysis on the slickensided surfaces. Deformation bands exhibiting reverse slip formed during the folding of SMA, probably during the later stages, while deformation bands exhibiting normal slip record post-folding extension of the basin rim.

ACKNOWLEDGMENTS

Associate Editor Terry Pavlis, E. Erslev, and an anonymous reviewer provided helpful reviews on an earlier draft of this manuscript. We thank Erslev for helpful conversations in the field, and C. Fretz, M. Alvarado, and D. Bammel for assistance in the collection of data in the field. M. Fan graciously shared microscopy facilities and offered helpful advice during the project. This work was supported by the American Chemical Society Petroleum Research Fund Grant 52300-UN18, a Geological Society of America Graduate Research Grant, and an American Association of Petroleum Geologists Southwest Section Graduate Research Scholarship.

REFERENCES CITED

Allmendinger, R., 2015, Stereonet: A computer program for plotting structural data on stereographic projections: Ithaca, New York, Cornell University Department of Earth and Atmospheric Sciences, http://www.geo.cornell.edu/geology/faculty/RWA/programs/stereonet.html.

Amrouch, K., Lacombe, O., Bellahsen, N., Daniel, J.-M., and Callot, J.-P., 2010, Stress and strain patterns, kinematics and deformation mechanisms in a basement-cored anticline: Sheep Mountain anticline, Wyoming: Tectonics, v. 29, TC1005, doi:10.1029/2009TC002525.

Atkinson, B., and Meredith, P., 1987, Experimental fracture mechanics data for rocks and minerals, *in* Atkinson, B., ed., Fracture Mechanics of Rock: London, Academic Press, p. 477–525, doi:10.1016/B978-0-12-066266-1.50016-8.

Aydin, A., and Johnson, A., 1978, Development of faults as zones of deformation bands and as slip surfaces in sandstone, *in* Byerlee, J.D., and Wyss, M., eds., Rock Friction and Earthquake Prediction: Contributions to Current Research in Geophysics 8: Basel, Birkhäuser, p. 931–942, doi:10.1007/978-3-0348-7182-2_23.

Barenblatt, G., 1962, The mathematical theory of equilibrium cracks in brittle fracture: Advances in Applied Mechanics, v. 7, p. 55–129, doi:10.1016/S0065-2156(08)70121-2.

Beaudoin, N., Leprêtre, R., Bellahsen, N., Lacombe, O., Amrouch, K., Callot, J.-P., Emmanuel, L., and Daniel, J.-M., 2012, Structural and microstructural evolution of the Rattlesnake Mountain Anticline (Wyoming, USA): New insights into the Sevier and Laramide orogenic stress build-up in the Bighorn Basin: Tectonophysics, v. 576, p. 20–45, doi:10.1016/j.tecto.2012.03.036.

Bellahsen, N., Fiore, P., and Pollard, D., 2006, The role of fractures in the structural interpretation of Sheep Mountain Anticline, Wyoming: Journal of Structural Geology, v. 28, p. 850–867, doi:10.1016/j.jsg.2006.01.013.

Bourne, S., 2003, Contrast of elastic properties between rock layers as a mechanism for the initiation and orientation of tensile failure under uniform remote compression: Journal of Geophysical Research, v. 108, 2395, doi:10.1029/2001JB001725.
Bourne, S., and Willemse, E., 2001, Elastic stress control on the pattern of tensile fracturing around a small fault network at Nash Point, UK: Journal of Structural Geology, v. 23, p. 1753–1770, doi:10.1016/S0191-8141(01)00027-X.
Bowles, J., 1996, Foundation Analysis and Design (fifth edition): New York, McGraw-Hill, 1201 p.
Braccini, E., de Boer, W., Hurst, A., Huuse, M., Vigorito, M., and Templeton, G., 2006, Sand injectites: Schlumberger Oilfield Review 20, p. 34–49.
Bureau, D., Mourgues, R., and Cartwright, J., 2014, Use of a new artificial cohesive material for physical modelling: Application to sandstone intrusions and associated fracture networks: Journal of Structural Geology, v. 66, p. 223–236, doi:10.1016/j.jsg.2014.05.024.
Bürgmann, R., Pollard, D., and Martel, S., 1994, Slip distributions on faults: Effects of stress gradients, inelastic deformation, heterogeneous host-rock stiffness, and fault interaction: Journal of Structural Geology, v. 16, p. 1675–1690, doi:10.1016/0191-8141(94)90134-1.
Byrd, J., Smith, R., and Geissman, J., 1994, The Teton fault, Wyoming: Topographic signature, neotectonics, and mechanisms of deformation: Journal of Geophysical Research, v. 99, p. 20,095–20,122, doi:10.1029/94JB00281.
Cooke, M., and Pollard, D., 1996, Fracture propagation paths under mixed mode loading within rectangular blocks of polymethyl methacrylate: Journal of Geophysical Research, v. 101, p. 3387–3400, doi:10.1029/95JB02507.
Cooke, M., and Underwood, C., 2001, Fracture termination and step-over at bedding interfaces due to frictional slip and interface opening: Journal of Structural Geology, v. 23, p. 223–238, doi:10.1016/S0191-8141(00)00092-4.
Cotterell, B., and Rice, J., 1980, Slightly curved or kinked cracks: International Journal of Fracture, v. 16, p. 155–169, doi:10.1007/BF00012619.
Crowley, P., Reiners, P.W., Reuter, J.M., and Kaye, G.D., 2002, Laramide exhumation of the Bighorn Mountains, Wyoming: An apatite (U-Th)/He thermochronology study: Geology, v. 30, p. 27–30, doi:10.1130/0091-7613(2002)030<0027:LEOTBM>2.0.CO;2.
Dahlstrom, C., 1969, The upper detachment in concentric folding: Bulletin of Canadian Petroleum Geology, v. 17, p. 326–346.
DeCelles, P., 2004, Late Jurassic to Eocene evolution of the Cordilleran thrust belt and foreland basin system, western USA: American Journal of Science, v. 304, p. 105–168, doi:10.2475/ajs.304.2.105.
Delaney, P., and Pollard, D., 1981, Deformation of host rocks and flow of magma during growth of minette dikes and breccia-bearing intrusions near Ship Rock, New Mexico: U.S. Geological Society Professional Paper 1202, 61 p.
Delaney, P., Pollard, D.D., Ziony, J.I., and McKee, E.H., 1986, Field relations between dikes and joints: Emplacement processes and paleostress analysis: Journal of Geophysical Research, v. 91, p. 4920–4938, doi:10.1029/JB091iB05p04920.
Demoulin, C., 1978, Clastic (Neptunian) dykes and sills, *in* Fairbridge, R.W., ed., Encyclopedia of Sedimentology: Springer Encyclopedia of Earth Science series, p. 217–219, doi:10.1007/3-540-31079-7_45.
Dickinson, W., Klute, M.A., Hayes, M.J., Janecke, S.U., Lundin, E.R., McKittrick, M.A., and Olivares, M.D., 1988, Paleogeographic and paleotectonic setting of Laramide sedimentary basins in the central Rocky Mountain region: Geological Society of America Bulletin, v. 100, p. 1023–1039, doi:10.1130/0016-7606(1988)100<1023:PAPSOL>2.3.CO;2.
Erslev, E., 1993, Thrusts, back-thrusts, and detachment of Rocky Mountain foreland arches, *in* Schmidt, C.J., et al., eds., Laramide Basement Deformation in the Rocky Mountain Foreland of the Western United States: Geological Society of America Special Paper 280, p. 339–358, doi:10.1130/SPE280-p339.
Fan, M., and Carrapa, B., 2014, Late Cretaceous–early Eocene Laramide uplift, exhumation, and basin subsidence in Wyoming: Crustal responses to flat slab subduction: Tectonics, v. 33, p. 509–529, doi:10.1002/2012TC003221.
Fan, M., and Dettman, D., 2009, Late Paleocene high Laramide ranges in northeast Wyoming: Oxygen isotope study of ancient river water: Earth and Planetary Science Letters, v. 286, p. 110–121, doi:10.1016/j.epsl.2009.06.024.
Fanshawe, J., 1971, Structural evolution of Big Horn basin, *in* Renfro, A.R., ed., Symposium on Wyoming Tectonics and their Economic Significance: Wyoming Geological Association 23rd Annual Field Conference Guidebook, p. 35–42.
Fisher, C., 1906, Geology and water resources of the Bighorn Basin, Wyoming: U.S. Geological Survey Professional Paper 53, 72 p., doi:10.5962/bhl.title.50789.
Forster, A., Irmen, A., and Vondra, C., 1996, Structural interpretation of Sheep Mountain Anticline, Bighorn Basin, Wyoming, *in* Resources of the Bighorn Basin: Wyoming Geological Association 47th Annual Field Conference Guidebook, p. 239–251.
Gale, J., Reed, R., and Holder, J., 2007, Natural fractures in the Barnett Shale and their importance for hydraulic fracture treatments: American Association of Petroleum Geologists Bulletin, v. 91, p. 603–622, doi:10.1306/11010606061.
Gercek, H., 2007, Poisson's ratio values for rocks: International Journal of Rock Mechanics and Mining Sciences, v. 44, p. 1–13, doi:10.1016/j.ijrmms.2006.04.011.
Griffith, W.A., Mitchell, T.M., Renner, J., and Di Toro, G., 2012, Coseismic damage and softening of fault rocks at seismogenic depths: Earth and Planetary Science Letters, v. 353–354, p. 219–230, doi:10.1016/j.epsl.2012.08.013.
Gudmundsson, A., 2002, Emplacement ad arrest of sheets and dykes in central volcanoes: Journal of Volcanology and Geothermal Research, v. 116, p. 279–298, doi:10.1016/S0377-0273(02)00226-3.
Hennier, J., 1984, Structural analysis of the Sheep Mountain anticline, Bighorn basin, Wyoming [M.S. thesis]: College Station, Texas A&M University, 118 p.
Hennier, J., and Spang, J., 1983, Mechanisms for deformation of sedimentary strata at Sheep Mountain anticline, Bighorn Basin, Wyoming, *in* The Bighorn Basin: Wyoming Geological Association 34th Annual Field Conference Guidebook, p. 96–111.
Hoy, R., and Ridgway, K., 1997, Structural and sedimentological development of footwall growth synclines along an intraforeland uplift, east-central Bighorn Mountains, Wyoming: Geological Society of America Bulletin, v. 109, p. 915–935, doi:10.1130/0016-7606(1997)109<0915:SASDOF>2.3.CO;2.
Hurst, A., and Cartwright, J., 2007, Relevance of sand injectites in hydrocarbon exploration and production, *in* Hurst, A., and Cartwright, J., eds., Sand Injectites: Implications for Hydrocarbon Exploration and Production: American Association of Petroleum Geologists Memoir 87, p. 1–19, doi:10.1306/1209846M871546.
Irwin, G., 1958, Fracture, *in* Flugge, S., ed., Handbuch der Physik: Berlin, Springer, p. 551–590.
Johnson, G., Garside, L., and Warner, A., 1965, A study of the structure and associated features of Sheep Mountain Anticline, Big Horn County, Wyoming: Iowa Academy of Science Proceedings, v. 72, p. 332–342.
Jolly, R., and Lonergan, L., 2002, Mechanisms and controls on the formation of sand intrusions: Journal of the Geological Society [London], v. 159, p. 605–617, doi:10.1144/0016-764902-025.
Kunkle, C., and Griffith, A., 2011, Deformation bands in large sandstone dikes near Sheep Mountain Anticline, North-central Wyoming: Geological Society of America Abstracts with Programs, v. 43, no. 1, p. 168.
Lachenbruch, A., 1961, Depth and spacing of tension cracks: Journal of Geophysical Research, v. 66, p. 4273–4292, doi:10.1029/JZ066i012p04273.
Lorenz, J., Teufel, L., and Warpinski, N., 1991, Regional fractures I: A mechanism for the formation of regional fractures at depth in flat-lying reservoirs: American Association of Petroleum Geologists Bulletin, v. 75, p. 1714–1737.
Love, J., 1960, Cenozoic sedimentation and crustal movement in Wyoming: American Journal of Science, v. 258, p. 204–214.
Mair, K., Elphick, S., and Main, I., 2002, Influence of confining pressure on the mechanical and structural evolution of laboratory deformation bands: Geophysical Research Letters, v. 29, no. 10, p. 49-1–49-4, doi:10.1029/2001GL013964.
Maltman, A., ed., 1994, The Geological Deformation of Sediments: London, Chapman and Hall, 362 p., doi:10.1007/978-94-011-0731-0.
Marrett, R., and Allmendinger, R., 1990, Kinematic analysis of fault-slip data: Journal of Structural Geology, v. 12, p. 973–986, doi:10.1016/0191-8141(90)90093-E.
Martel, S., 1997, Effects of cohesive zones on small faults and implications for secondary fracturing and fault trace geometry: Journal of Structural Geology, v. 19, p. 835–847, doi:10.1016/S0191-8141(97)00002-3.
McMillan, M., Heller, P., and Wing, S., 2006, History and causes of post-Laramide relief in the Rocky Mountain orogenic plateau: Geological Society of America Bulletin, v. 118, p. 393–405, doi:10.1130/B25712.1.
Pollard, D., and Aydin, A., 1988, Progress in understanding jointing over the past century: Geological Society of America Bulletin, v. 100, p. 1181–1204, doi:10.1130/0016-7606(1988)100<1181:PIUJOT>2.3.CO;2.

Pollard, D., and Muller, O., 1976, The effect of gradients in regional stress and magma pressure on the form of sheet intrusions in cross section: Journal of Geophysical Research, v. 81, p. 975–984, doi:10.1029/JB081i005p00975.

Pollard, D., Segall, P., and Delaney, P., 1982, Formation and interpretation of dilatant echelon cracks: Geological Society of America Bulletin, v. 93, p. 1291–1303, doi:10.1130/0016-7606(1982)93<1291:FAIODE>2.0.CO;2.

Ray, R., and Keefer, W., 1985, Wind River basin, central Wyoming, *in* Gries, R.R., and Dyer, R.C., eds., Seismic Exploration of the Rocky Mountain Region: Denver, Colorado, Rocky Mountain Association of Geologists, p. 201–217.

Rodrigues, N., Cobbold, P., and Løseth, H., 2009, Physical modelling of sand injectites: Tectonophysics, v. 474, p. 610–632, doi:10.1016/j.tecto.2009.04.032.

Rowe, C.D., Kirkpatrick, J.D., and Brodsky, E.E., 2012, Fault rock injections record paleoearthquakes: Earth and Planetary Science Letters, v. 335–336, p. 154–166, doi:10.1016/j.epsl.2012.04.015.

Rubin, A., 1993, Tensile fracture of rock at high confining pressure: Implications for dike propagation: Journal of Geophysical Research, v. 98, p. 15,919–15,935, doi:10.1029/93JB01391.

Rubin, A., 1995, Propagation of magma-filled cracks: Annual Review of Earth and Planetary Sciences, v. 23, p. 287–336, doi:10.1146/annurev.ea.23.050195.001443.

Simonson, E., Abou-Sayed, A., and Clifton, R., 1978, Containment of massive hydraulic fractures: Society of Petroleum Engineers Journal, v. 18, p. 27–32, doi:10.2118/6089-PA.

Smart, P., et al., 1988, Neptunian dikes and fissure fills: An overview and account of some modern examples, *in* James, N.P., and Choquette, P.W., eds., Paleokarst: New York, Springer, p. 149–162, doi:10.1007/978-1-4612-3748-8_8.

Stanton, H., and Erslev, E., 2002/2003, Sheep Mountain: Backlimb tightening and sequential deformation in the Bighorn Basin, Wyoming, *in* Wyoming Basins: Wyoming Geological Association 53rd Annual Field Conference Guidebook, p. 75–87.

Tada, H., Paris, P., and Irwin, G., 1985, The Stress Analysis of Cracks Handbook: St. Louis, Paris Productions Inc.

Talbot, C., and von Brunn, V., 1989, Melanges, intrusive and extrusive sediments, and hydraulic arcs: Geology, v. 17, p. 446–448, doi:10.1130/0091-7613(1989)017<0446:MIAESA>2.3.CO;2.

Thomas, L., 1965, Sedimentation and structural development of Big Horn basin: American Association of Petroleum Geologists Bulletin, v. 49, p. 1867–1877.

Vigorito, M., and Hurst, A., 2010, Regional sand injectite architecture as a record of pore-pressure evolution and sand redistribution in the shallow crust: Insights from the Panoche giant injection complex, California: Journal of the Geological Society [London], v. 167, p. 889–904, doi:10.1144/0016-76492010-004.

Warner, A., 1968, The description and origin of the clastic dikes associated with Sheep Mountain Anticline in the Bighorn Basin, Wyoming [M.S. thesis]: Ames, Iowa State University, 96 p.

Warpinski, N., and Teufel, L., 1987, Influence of geologic discontinuities on hydraulic fracture propagation (includes associated papers 17011 and 17074): Journal of Petroleum Technology, v. 39, no. 02, p. 209–220, doi:10.2118/13224-PA.

Willemse, E., and Pollard, D., 1998, On the orientation and patterns of wing cracks and solution surfaces at the tips of a sliding flaw or fault: Journal of Geophysical Research, v. 103, p. 2427–2438, doi:10.1029/97JB01587.